POLITECNICO DI TORINO

Master of Science in Building Engineering

MASTER'S DEGREE THESIS

A comprehensive approach about the cracks in post-tensioned bridges and case study .

Supervisor:

Prof. Eng. Marco Domaneschi

Co-supervisors:
Eng. Rebecca Asso
Eng. Mattia Mairone
Eng. Davide Masera, Phd

Candidate:

Ali Jouni

Abstract:

Post-tensioned bridges are a type of bridge construction that utilizes high-strength steel tendons or cables within the concrete structure. These tendons are tensioned after the concrete has set, applying compressive forces to the concrete, which enhances its strength and durability. Post-tensioned bridges are often preferred for their ability to span longer distances and carry heavier loads compared to traditional bridges, making them suitable for various transportation infrastructure projects such as highways, railways, and pedestrian bridges.

This thesis delves into a comprehensive investigation of the occurrence and behavior of cracks specifically in post-tensioned bridges, with a primary focus on the critical aspect of structures subjected to tensioning forces. Through the use of finite element analysis, the study seeks to simulate and analyze the intricate processes involved in the formation and propagation of cracks within various components of post-tensioned bridge systems.

By adopting a simulation approach, this research aims to significantly enhance our understanding of how cracks develop under diverse loading conditions, thereby enabling a more precise assessment of the structural performance and safety of post-tensioned bridges. The utilization of advanced computational techniques allows for an in-depth exploration of the complex interactions between design parameters, construction practices, material properties, and external forces, all of which influence crack initiation and propagation.

The insights garnered from these simulations offer invaluable contributions to elucidating the underlying mechanics of cracks in post-tensioned bridges. Such knowledge is instrumental in informing the development of effective strategies for the design, maintenance, and rehabilitation of these critical infrastructure assets. By leveraging these insights, engineers and practitioners can make informed decisions to enhance the resilience and longevity of post-tensioned bridge structures, thereby ensuring the safety and reliability of transportation networks on a global scale.

Acknowledgment

1   RESEARCH PROPOSAL:

1.1   Introduction:

Bridges, the vital lifelines of modern transportation networks, stand as remarkable feats of engineering prowess. Their intricate designs and structural integrity facilitate the seamless movement of people and goods, underpinning economic activities and societal connectivity. However, the stability and reliability of these essential infrastructure elements are not without their vulnerabilities. Among the numerous challenges that bridges face, cracks emerge as a critical concern, capable of triggering a cascade of consequences that extend beyond mere physical damage. As bridges play an irreplaceable role in sustaining economies and ensuring public safety, understanding the intricacies of cracks within the context of post-tensioned bridges becomes paramount.

When a bridge succumbs to failure, the repercussions extend far beyond its immediate physical collapse. The aftermath reverberates through economic, social, and safety dimensions, creating a domino effect that can be felt across a wide spectrum. This ripple effect, often underestimated, emphasizes the dire need for a comprehensive understanding of the causes and implications of cracks within post-tensioned bridges. By unraveling the underlying mechanisms that lead to crack formation and propagation, we can bolster the resilience of these critical structures and safeguard the well-being of societies they serve.

In light of the multifaceted nature of bridge failures, this thesis embarks on an exploration into the realm of cracks within post-tensioned bridges. Our endeavor seeks to uncover the intricate interplay of factors contributing to crack development, aiming to shed light on their implications for structural integrity, safety, and economic stability. Through an analysis of historical cases, advanced testing methodologies, and a deep dive into structural engineering principles, we aim to forge a comprehensive understanding of cracks within post-tensioned bridges and pave the way for enhanced assessment, management, and mitigation strategies.

The following chapters will delve into a systematic investigation of crack formation, propagation, and their effects on post-tensioned bridges. By elucidating the complex dynamics of cracks, we aspire to contribute to the body of knowledge that guides the design, maintenance, and management of these critical components of our built environment. As we navigate through this research journey, we remain cognizant of the profound impact that our findings can have on ensuring the longevity, safety, and functionality of bridges, thereby fostering resilient and sustainable societies.

1.2 Research purpose:

This paper attempts to document those types of problems that lead to cracking in post-tensioned concrete box girder bridges and have been encountered in both Europe and the United States.

These problems are not limited to those of prestressed box girder bridges, but may occur in other types of structures with similar conditions and details.

The surveys conducted on bridge failures have revealed a wide range of causes, including accidents, natural catastrophes, external events, construction deficiencies, and corrosion. Moreover, these causes have been found to be significantly influenced by various characteristics of the bridge, such as its location, environment, age, and structural typology.

Due to the diverse factors contributing to bridge failures and the varying conditions in different regions, each country has directed its research efforts towards understanding the specific characteristics and conditions relevant to their territory. This approach allows them to address the unique challenges and potential vulnerabilities of their bridges effectively, aiming to improve the overall safety and durability of their transportation infrastructure.

1.3   Research Methodology:

Post-tensioned bridges play a vital role in modern transportation infrastructure, providing efficient and durable solutions for spanning vast distances. However, as these bridges age and endure various environmental and loading conditions, the emergence of cracks becomes a concerning issue. Cracks in post-tensioned bridges can lead to significant economic losses, compromise structural integrity, and pose potential risks to public safety.

This research aims to address the critical challenges posed by cracks in post-tensioned bridges through a comprehensive investigation. The study seeks to explore the underlying causes, assess the extent and severity of cracking, analyze its impact on structural performance, and identify effective strategies for prevention and repair. By addressing these research questions, the study aims to contribute to improved understanding, maintenance, and design practices, ultimately enhancing the safety, durability, and reliability of post-tensioned bridges in transportation networks.

The research will begin with an extensive literature review, delving into existing studies, technical reports, and industry standards that highlight the causes and implications of cracks in post-tensioned bridges. This review will serve as the foundation for formulating research questions that address the multifaceted aspects of the issue.

Through data collection, quantitative and qualitative approaches will be employed to gather information from bridge inspection reports, monitoring data, and expert interviews. The collected data will then be subjected to crack detection and analysis using non-destructive testing methods and finite element analysis to understand the characteristics, size, and distribution of cracks and their effects on the structural behavior of post-tensioned bridges.

The research will also include in-depth case studies of real-world instances of post-tensioned bridges with cracks. These case studies will provide practical insights into the challenges faced by engineers and the effectiveness of different repair and prevention approaches.

Ultimately, the research aims to offer valuable recommendations and best practices for bridge engineers and policymakers. The proposed guidelines will encompass preventive maintenance strategies, crack detection methods, and repair techniques, empowering stakeholders to make informed decisions to ensure the long-term performance and safety of post-tensioned bridges in transportation infrastructure. By addressing these research questions comprehensively, this study seeks to advance knowledge in the field and contribute to the sustainable and resilient development of transportation networks.

1.4 *Main objectives & sub-objectives:*

Post-tensioned bridges are essential components of transportation infrastructure, providing efficient transportation across significant spans. However, over time, these bridges may develop cracks, which can potentially compromise their structural integrity and safety. This research aims to investigate the causes, extent, and potential mitigation strategies for cracks in post-tensioned bridges.

. **Research Objectives:**
- To identify the common causes of cracks in post-tensioned bridges.
- To assess the severity and extent of cracks in various post-tensioned bridge structures.
- To analyze the impact of cracks on the overall structural performance and safety of the bridges.
- To explore effective mitigation techniques and maintenance strategies for addressing cracks in post-tensioned bridges.

1.5   *Research question:*

This research focuses on investigating the phenomenon of cracks in post-tensioned bridges to gain a deeper understanding of its causes, extent, and potential solutions.

- What are the common causes of cracks in post-tensioned bridges, and how do they vary based on factors such as bridge age, design, and environmental conditions?

- How do the characteristics of cracks (e.g., length, width, depth) in post-tensioned bridges differ from those in conventionally reinforced bridges?

- What non-destructive testing methods are most effective in detecting and monitoring cracks in post-tensioned bridge structures, and how can they be optimized for accurate assessments?

2   LITERATURE REVIEW

2.1   Cracks in post-tensioned

Cracking in post-tensioned concrete box girders generally results, in a broad sense, for the following reasons: inadequate flexural and shear capacity, nonconsideration of thermal stresses, insufficient attention to stresses developed by curvature of tendons, improper or inappropriate construction techniques, lack of quality workmanship to meet the tolerances necessary for problem free structures, and under-strength materials.(Podolny, 1985)

❖ FLEXURAL CRACKING

Flexural cracking is associated with tensile stresses that exceed the tensile capacity of concrete. They are generally found, in continuous girders, at the bottom of the girder in positive moment areas and at the top of the girder in negative moment areas.

In areas near the support the effect of shear will be superimposed producing,cracks that are inclined and become more and more diagonal in the webs, which may indicate insufficient shear strength

Cracks of this type pose a risk to the reinforcement, prestress or conventional, that traverse the crack from corrosion or from fatigue damage under large and frequent stress variation.
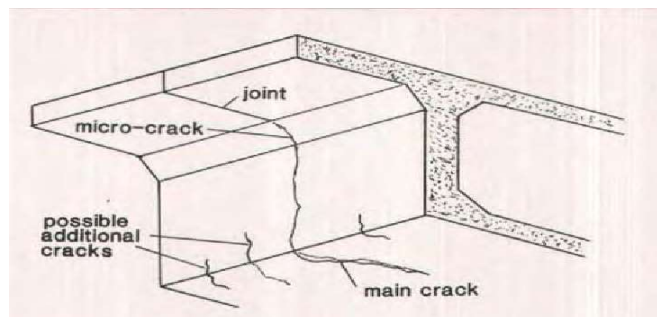
Figure 1-Cracks (Podolny, 1985)

The more prevalent causes are as follows:

o   During design:
➢   Inadequate consideration of, or underestimation of, stresses resulting from moment redistribution.
➢   Underestimation of thermal stresses (expansion or contraction),
➢   Lack of consideration of, or underestimation of, thermal gradient.
➢   Overestimation of initial prestress resulting from optimistic coefficients of friction and wobble.
➢   Underestimating relaxation loss inprestressing.
➢   Selection of a tendon profile whereby a large variation of prestress eccentricity occurs.
o   During construction:

➤ Losses because of excessive friction resulting from crushed tendon ducts.
➤ Displacement of poorly secured tendon ducts which then alters the eccentricity and also produces additional friction.
➤ Lack of isolation from the concrete of tendon couplers. If the coupler is positioned such that it cannot freely move as the tendon elongates under stressing, the prestress force distribution is altered.
➤ Failure of strands or wires in a tendon.

o **Excess permanent load:**
➤ Underestimating the weight of construction equipment and permanent nonstructural loads.
➤ Accidental displacement of forms before or during concrete placement resulting in a greater thickness and heavier deck.
➤ Underestimation of the voiuminal mass of concrete, especially where dense aggregates such as those of basaltic origin are used.

o **Secondary stresses and overloads :**
These are stresses experienced during construction and service life for which it may not have been designed.

➤ Differential settlement of supports or movements of pier foundations which modify stresses and/or deformations.
➤ Overload from heavy truck traffic and accompanying dynamic effects.
➤ Failure to recognize local effects such as, for example, curvature of tendons or stresses behind anchorages.

❖ **SHEAR CRACKING**
Shear cracks occur in the webs and are perceptibly inclined at approximately a 45 deg angle. They normally manifest themselves in a zone between the support and an inflection point.
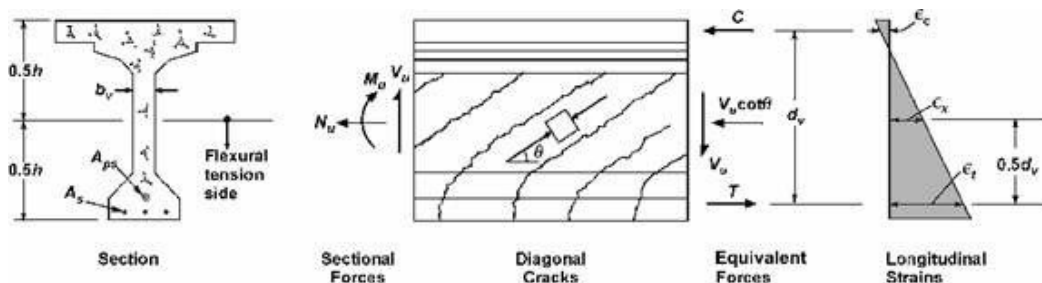
Figure 2-Shear cracking.

■ Most of the causes of flexural cracks are also responsible for shear cracks since a change in bending moment automatically changes shear stress:

➢ Insufficient prestressing
➢ Excess permanent loads
➢ Secondary stresses
➢ Thermal effects

■ Shear cracks can also be initiated by bending cracks or high tensile stresses behind tendon anchorages. The following design oversights may also contribute to the formation of shear cracks:

➢ Failure to recognize the effect of inclination of continuity tendons in variable depth girders. Although the vertical component of a single tendon may be small, if there are a large number of tendons they can create a significant shear force.

❖ Cracking produced by incorrect distribution of forces :

A complete investigation of the problems encountered revealed that cracking was the result of the superposition of several adverse effects, any of which might have been harmless if considered

separately:

➢ failed to take into account the curvature of continuity tendons distributed in the bottom flange is
➢ such that a downward reaction is produced at the webs that is additive to the shear in the web.
➢ The distribution of shear stresses was made under the conventional structural analysis assumption that the cross section was rigid and transversely undeformable.
➢ The vertical web prestress was partially lost into the intermediate diaphragms, and the actual vertical compressive stress was lower than assumed.

❖ THERMAL STRESS CRACKING

■ The current AASHTO Specifications° recognize thermal expansion and contraction in the design of bridge structures. The rise and fall of temperature should be determined for the site of the structure under consideration. In general, AASHTO requirements for temperature rise and fall of a concrete structure about an assumed temperature at time of construction is as follows:

➢ The change in length of an unrestrained member can be determined. Where a member is restrained (fixity of supports or friction in bearings) the thermal expansion or contraction is prevented by reactions at the supports which then cause stresses in the member. This stress is calculated by

assuming that the thermal expansion or contraction first occurs and then forces (reactions) are applied at the restraints to bring the member hack to its original length.

- Bridge engineers have relatively recently become aware of another thermal phenomenon, namely, thermal gradient. As a result of the poor thermal conductivity of concrete, a temperature gradient will occur through the depth of a concrete member.

➤ The gradient is a function of a number of variables such as :
  solar radiation, ambient temperature, wind speed fluctuations, material properties, surface characteristics, and section shape. This type of thermal gradient will cause external restraint forces in statically indeterminate structures such as continuous girders.

➤ In prestressed concrete structures there may be zones, under dead load plus prestress, where there is a low compressive stress reserve and the stresses due to restraint forces can easily reach values that exceed the tensile strength of the concrete.

➤ This usually leads to vertical cracks very close to intermediate supports. Cracking as a result of thermal gradients have been re ported13 and is considered to he one of four prime causes of cracking in prestressed concrete bridges.In some cases the thermal gradient stresses can be larger than the live load stresses.These cracks can be further enhanced aggravated by stresses resulting from bearing pressure at the supports or radial tendon stresses from curved ten dons in the support area.

➤ The effects of thermal gradient are usually computed by assuming the gradient to be constant throughout the bridge superstructure length.

- Another source of thermal stress (strain) related cracking is that associated with heat of hydration, subsequent cooling and shrinkage. Heat of hydration is a chemical process that is a function of the type and amount of cement, thickness of concrete members and temperature of aggregate.

➤ Thin parts of the cross section will cool faster than adjoining thick parts producing residual tensile stress and cracking,thus the thinner member will crack.

➤ To relieve tensile strains, produced by restraint of the webs, the thin bottom flange has no other alternative but to crack . In a transverse section, large differences in thickness can produce restraining moments which can produce horizontal cracks in the webs.

➤ Usually, because of insufficient longitudinal reinforcement and/or lack of sufficient bond development between the reinforcement and the young concrete, there is insufficient capacity for

the younger concrete to resist the restraint to shrinkage produced by the older concrete and cracking of the younger concrete will occur. If the forms are left in place too long, they will present large surface area of friction that will also hamper the shrinkage of the new concrete and thus cause cracking.

❖ CRACKING AT/OR NEAR ANCHORAGES

Certain anchorage positions, such as an anchorage blister on a thin flange , should be avoided.

Wherever possible, anchorage blisters for continuity tendons should be placed in a fillet between the web and flange where the transverse section has the largest rigidity. If this type of detail cannot be avoided, then particular attention must he paid in design and construction to the zone concerned.

Cracking will originate in the bottom flange behind continuity anchorage blisters and propagate forward toward the webs, along a line forming a 30 to 45 deg angle with the longitudinal axis of the girder . If the rear face of the blister is located in close proximity to a segment joint, cracking may develop in the joint . In some situations the diagonal or herringbone cracks in the bottom flange continue to propagate to the webs forming a 30 to 45 deg angle with a horizontal axis.

The truss analogy indicates clearly that such tensile stresses are superimposed on the normal shear and diagonal stress due to the applied dead load and may therefore produce cracking. This could have been prevented by extending the vertical prestress in the webs further out toward midspan. The cause of this type of cracking is the application of a tendon force to a small area of slab, in its plane, compressing the slab forward of the force in a zone of radial compression stresses that cause tensile stresses behind the point of application of the tendon force.

❖ Among the parameters that can produce this type of cracking are the following:

1. Termination of numerous continuity tendons in a single section, particularly when the joint behind the anchorages is not compressed by other tendons.

2. Insufficient horizontal offset between tendon anchorages in the top and bottom flanges.

<u>Aprroach :</u>

If this type of cracking or failure is to be inhibited, the design, detailing, and placement of reinforcement in these highly stressed zones must be carefully considered. Location of blisters must be considered and there must he sufficient longitudinal reinforcement behind the blister or anchorage and sufficient transverse reinforcement abreast of the anchorage to accommodate the initial tendon forces. In a recent failure of this type, after epoxy injection of the cracks, additional external post-tensioning was provided to close-up and induce compression in open segment joints and cracks

❖ <u>CRACKS RESULTING FROM VERTICAL CURVATURE OF SOFFIT TENDONS</u>

This type of distress is associated with variable depth girders and occurs in the positive moment area. It is manifested by longitudinal cracks occurring in the bottom flange, at the juncture of the bottom flange and web, and possibly in the web.

Therefore, the effect of tendon curvature adds fully to the dead load stresses of the concrete flange. The corresponding flexural stresses may be four to five times greater than the effect due to dead load only, and if sufficient reinforcement is not provided for this effect, heavy cracking is to be expected and possibly failure. Practically, this situation may be aggravated by tendon cusps associated with tendon profile deviations which will be subsequently discussed.

❖ <u>CRACKS RESULTING FROM CORROSION</u>

Accurate prediction of corrosion product volume and distribution in steel rebars is essential for estimating concrete behavior in extreme environmental circumstances. Corrosion-induced stresses can lead to crack formation, reducing the bearing capacity of concrete structures. Research efforts have resulted in advanced models for predicting the effects of corrosion, which have improved the understanding of vulnerability in concrete structures. The corrosion process not only reduces durability but also causes diverse degradation mechanisms, including a decrease in cross-sectional area, bond strength, and mechanical properties of concrete. (Soltani & al., 2022)

o <u>Review of corrosion distribution models</u>

The nonuniform distribution concept, which is closer to the nature of the corrosion phenomena, has been utilized in advanced predicting models. In the following, the common models for each concept are reviewed.

o <u>Nonuniform-based models</u>

Yuan and Ji conducted a comprehensive investigation on the nonuniform distribution of corrosion products (CPD) in 2009, using high-precision surface imaging techniques. Their results demonstrated

higher CPD in the concrete cover, especially the backside. Building on this research, Ning Xia et al. proposed a statistical model in trigonometric function form for predicting the distribution of iron rust, while Pan and Lu used a quadratic parabolic distribution to describe the radial volume of CPD. Additionally, K.K. Tran developed a model that considered a uniform CPD on the rebar's perimeter before crack formation, with a 0.1 mm opening. However, this uniform distribution was assumed only on half or a quarter of the circumference within the cracks. Assessment of CPD models.

- Calculation of the CP volume per unit thickness

$$Vrust = t \int_0^{2\pi} Tcl(\theta).r d\theta = t \sum Tcl.r.\delta\theta$$

- volumetric expansion coefficient

$$\Omega = \frac{Vrust}{Vcs} = \frac{\int_0^{2\pi} Tcl(\theta).r.d\theta}{\rho.\pi.r2} = \frac{\sum Tcl.r.\delta\theta}{\rho.\pi.r2}$$

- Tcl → the total thickness of CP
- R → steel rebar radius
- θ → angle in radians
- ρ → corrosion percentage of steel rebars
- Vrust → the iron rust volume
- Vcs → the corroded steel volume
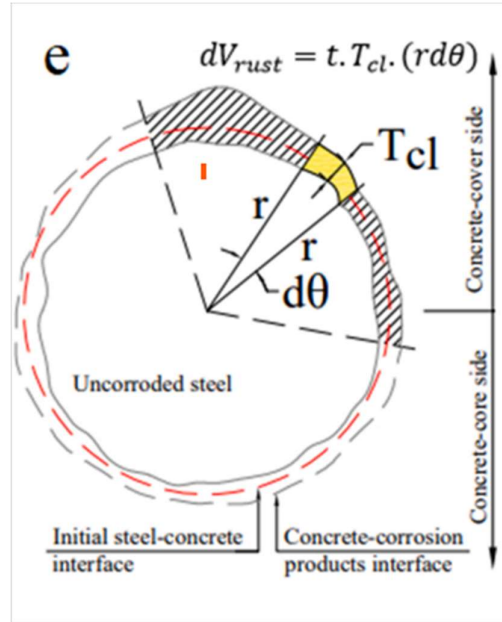
Figure 3-(Soltani & al., 2022)

2.2 The NDE methods for the external tendon system are introduced below(Hurlebaus & al., 2016)

❖ Electromagnetic Methods

o Ground Penetrating Radar

Ground Penetrating Radar (GPR) can detect voids inside HDPE ducts, but it is not effective when metallic materials are present, as they cause distortions in the results.

o Infrared Thermography

Infrared techniques, both active and passive, have been used to locate voided regions in internal ducts with shallow concrete cover.Active Infrared Thermography (IRT) is expected to be useful in locating defects in external ducts.

❖ Radiography
- X-ray radiography, which was discussed for internal PT tendons, can also be used to evaluate external tendons if access to the duct is available.
- Gamma-ray Radiography. The same use of gamma-ray radiography in the discussion for the internal PT tendons can be used to effectively evaluate external tendons provided access to the duct is available. Like x-ray, gamma-ray radiography is expensive, requires massive shielding, and requires two-sided access
- Computed Tomography (CT) has been used to examine a sample specimen with three strands within grouted ducts (Im et al. 2010b).The CT imaging revealed the presence of voids inside the duct.However, the observed size of the voids may be affected by beam hardening in high-density materials.CT is capable of producing detailed images of the structure.However, CT devices are expensive, and they require accessibility to the concrete specimen from both sides, which limits their practical application in the field.

❖ Elasto-Magnetic (EM) Method
The elasto-magnetic (magneto-elastic) technique was initially developed to estimate stress in cables and can identify stress changes and section loss caused by corrosion.The technique is based on the concept that magnetic permeability is sensitive to stress variations.The EM sensors effectively monitored stress loss due to factors such as shrinkage, relaxation, creep, and elastic deformation.

❖ Electrical Capacitance Tomography (ECT)
Electrical Capacitance Tomography (ECT) has been used to reconstruct cross-sectional images of oil flow in non-conductive pipelines.ECT utilizes multi-electrode sensors to obtain capacity data and iteratively generates permittivity images of sections.These images can reveal the presence of air pockets in oil flow.

❖ Magnetic Methods (Magnetic Flux Leakage)
Azizinamini and Gull (2012) identified the MFL techniques as one of the most promising methods for detecting damage in external PT tendons.

- Active Magnetic Flux Leakage,The experiments used concrete and wood-framed housings to mimic internal PT tendons, but the technique could be modified for external tendons and guided by a robot.The MFL technique was tested on metal ducts and considered the presence of longitudinal and transverse reinforcement surrounding the ducts.The researchers believed that such a device could be adapted for use with external tendons.
- Residual Magnetic Flux Leakage (or Remanent Magnetic Flux Leakage),It was reported that applying the passive MFL method was successful in the detection of corroded external tendons (Hillemeier and Scheel 1998; Tilly 2002). As with the active MFL approach, the MFL technique is effective in

detecting corrosion in metallic materials but cannot detect other discontinuities such as voids and cracks.

❖ <u>Mechanical Wave and Vibration Methods</u>

● The acoustic emission technique has been applied to external tendons in a PT bridge in order to monitor strand failures (Paulson et al. 2001). The AE sensors were attached to HDPE ducts near anchorages and deviator blocks in the bridge.

● The ultrasonic guided wave has proven to be a promising method for assessing the condition of external tendon systems (Beard et al. 2003; Chaki and Bourse 2009; Jezzine et al. 2009; Rizzo et al. 2007). In the experiments conducted, the application of UGW identified strand defects such as corrosion, fracture, and stress loss. Na et al. (2005) employed electro-magnetic acoustic 59 transducers (EMATs) to identify voids inside steel pipes (Na and Kundu 2002; Na et al. 2005). They successfully detected voids and other inclusions in the steel pipe specimens.

● Vibration response is a technique in which an external tendon (or stay cable) is impacted with a dead-blow hammer and accelerometers at fixed locations record the vibrational modes. Using FFT, and modeling the response as a dynamic system, it is possible to estimate the tension forces in the tendon

● For the inspection of external PT ducts, a sounding inspection is generally performed to identify the existence of voids in ducts. In the regular inspection of PT bridges, the sounding inspection is executed by tapping an impactor or coin and inspectors document tendons for further inspection using a borescope when tendons result in "irregular sounding" by tapping (Corven Engineering 2001; Trejo et al. 2009c).

❖ <u>Visual Methods</u>

Visual inspection is the most common and applied method of evaluation for external PT tendons. Inspectors are trained to keep a detailed account regarding the physical changes a structure develops.

❖ <u>Electrochemical Methods</u>

All electrochemical methods discussed in the internal PT tendon section are applicable to external systems and subject to the same challenges (access to steel, etc.).

Electrochemical Impedance Spectroscopy (EIS) is a technique that provides precise kinetic and mechanistic information using different methods and output formats. It can be utilized as an alternative method for studying corrosion, semiconductors, batteries, electroplating, and elector-organic synthesis. EIS offers valuable insights into the electrochemical processes and behaviors of various systems. (Reference: Orazem and Tribollet, 2008)

Summary :

NDE technologies	Defects				
	Corrosion	Section loss	Breakage	Compromised grout	Voids
GPR	No	No	No	Possible	Possible in plastic
IRT	Indirectly possible	Possible	Possible	Possible	Possible
Radiography	Possible	Yes	Yes	Possible	Possible
CT	Possible	Yes	Yes	Possible	Possible
EM	Yes	Yes	Yes	No	No
ECT	No	No	No	Yes	Yes
MFL	Yes	Yes	Yes	No	No
AE	Possible	Possible	Yes	No	No
US	Indirectly possible	Yes	Yes	Need to check	Yes
IR	Indirectly possible	Indirectly possible	Indirectly possible	Indirectly possible	Indirectly possible
Sounding	No	No	No	Need to check	Yes
Electro-chemical*	Possible	Possible	Possible	No	No
TDR*	Indirectly possible	Yes	Yes	Possible	Possible
FOS*	Indirectly possible	Possible	Possible	Possible	Possible
UGW*	Indirectly possible	Possible	Possible	No	No

Table 1 NDE Technologies for assessing conditions of external tendon systems.

2.3   *Evaluate Concrete Cracks*

Concrete structures frequently exhibit cracking, a phenomenon that can arise from factors like plastic shrinkage, constructional shifts, overloading, or creep. Additionally, chemical processes like alkali-aggregate reactions and corrosion can trigger crack formation. Both material and structural engineers are invested in comprehending the primary causes of concrete cracks and assessing the magnitude and seriousness of preexisting ones. Engineers commonly rely on two criteria to define cracks: their width and depth. This article will examine three techniques employed by engineers to assess the depth of cracks within concrete. (PrimeC. (2017, May 31))

How To Evaluate Concrete Cracks ?

Initiating visual examination and surveillance stands as the initial stride in comprehending the characteristics of prevailing cracks and their fundamental origins. For instance, slanted cracks along concrete beams proximate to their supports might indicate shear strain, while cracks displaying rust traces could stem from steel deterioration. Ordinarily, crack widths serve as indicators for gauging the gravity of concrete cracks, whereas crack depth serves the purpose of appraising the holistic structural soundness of the component.
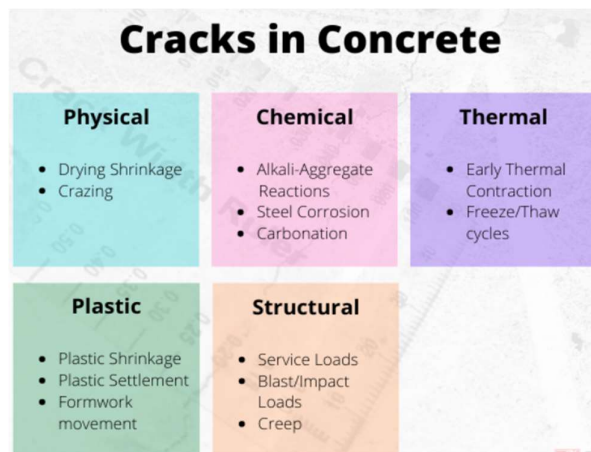
Figure 4- Cracks in concrete.

1. Crack Width

The assessment of crack intensity on the exterior of concrete typically involves the utilization of a crack width measuring tool, commonly referred to as a crack gauge. By considering the aperture of cracks visible on the surface, cracks can be characterized as minimal, akin to a hairline, or substantial, with openings spanning a few millimeters.

2. Crack Depth

Instances arise in which structural engineers prioritize the assessment of crack depth. The measurement of crack depth serves the purpose of appraising the robustness of the structure and confirming its long-lasting viability. Moreover, this measurement assists repair contractors in determining the expenses associated with remedial measures.

Diverse intrusive and non-intrusive methodologies are employed by engineers based on the project's characteristics to gauge crack depth.

Crack Depth Measurement in Concrete

I. Visual Examination of Concrete Cores

The extraction of core specimens from flaws is widely favored by inspectors and engineers as a prevalent technique. Depending on the crack's attributes and its placement (particularly if it lies within a critically compromised zone or in proximity to post-tensioning cables), core samples furnish insights regarding the range, profundity, and seriousness of cracks.

One approach involves the direct retrieval of cores, followed by a visual scrutiny of both the corehole and the core to discern potential triggers of the crack. In an alternative method, dye is forcefully introduced into surface cracks, subsequent to which concrete cores are extracted from the specified investigation area. These samples are then subject to microscopic analysis to ascertain the depth of concrete cracks.

Figure 5- Corehole.

II. Impact-Echo Method

The Impact-Echo test involves the generation of a stress pulse on the surface of a structure. This pulse propagates through the material and interacts with cracks, imperfections, and interfaces within the tested object. The response at the surface, triggered by the arrival of these reflected waves, is meticulously monitored using a high-precision receiving transducer (Malhotra and Carino, 2004). As stress waves traverse the concrete component, a portion of the acoustic waves emitted by the initial stress pulse at the surface reflects at the boundaries where there are variations in material stiffness.

The information captured by the transducer is typically subjected to frequency domain analysis to determine the velocity of the waves and the thickness of the material. This procedure has been standardized as ASTM C1383, titled "Standard Test Method for Measuring the P-Wave Speed and the Thickness of Concrete Plates Using the Impact-Echo Method".

The Impact-Echo technique finds utility in evaluating the depth of surface cracks. For this purpose, a specialized setup involving two transducers is required for conducting the impact-echo test.
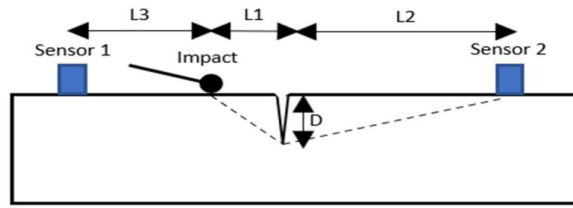
$$D = \sqrt[2]{\left[\frac{(V_P \times \Delta t)^2 + {L_1}^2 - {L_2}^2}{2 \times V_P \times \Delta t}\right]^2 - {L_1}^2}$$

Figure 6- Corehole.

In this context, where L1 signifies the separation between the horizontal point of impact and the crack, L2 represents the gap between the second sensor and the surface-exposed crack, and L3 depicts the interval between the impact point and the first sensor. VP stands for the velocity of the P-wave, while Δt refers to the time taken by the P-wave to travel from the initial impact to its detection at transducer 2.

III. Ultrasonic Pulse Velocity (UPV)

Ultrasonic Pulse Velocity (UPV) serves as a valuable non-destructive assessment technique for evaluating the integrity of concrete materials and identifying structural impairments. While UPV methods have traditionally been applied to quality control of materials, particularly homogeneous substances like metals and welded connections, recent strides in transducer technology have led to the widespread adoption of this test for appraising concrete materials.

Ultrasonic testing of concrete stands as an efficacious approach for gauging quality, ensuring uniformity, and estimating crack depths. The testing procedure has been standardized under the title "Standard Test Method for Pulse Velocity through Concrete" (ASTM C 597, 2016).

Figure 7- Ultrasonic testing.

For further insights into the UPV technique and its practical uses, you can access additional information by clicking here. The UPV method is applicable for determining the extent of surface cracks. To accomplish this, position each transducer on opposite sides of the crack, maintaining a specific distance. Subsequently, alter the distance between the transducers along the same path. The UPV measurement is then iterated across various transducer spacing intervals.

2.4   *Failure categorization*

The timing of damage detection in post-tensioned bridges is a critical aspect to ensure their safety and prevent potential failures. Early detection of damage allows engineers and maintenance personnel to address issues promptly and implement necessary repairs, minimizing the risk of further deterioration and ensuring the continued functionality of the bridge. Here are some key aspects of timing in damage detection for post-tensioned bridges:(Zhang & al., 2022)

❖ Regular Inspections

Post-tensioned bridges should undergo regular inspections at predetermined intervals, as part of routine maintenance and monitoring programs. These inspections can vary from visual assessments to more advanced non-destructive testing methods. The frequency of inspections depends on factors such as bridge age, usage, environmental conditions, and previous maintenance history.

❖ Real-Time Monitoring

Advancements in technology have enabled the implementation of real-time monitoring systems for post-tensioned bridges. These systems continuously collect data on bridge behavior, including strains, displacements, and temperature variations. Real-time monitoring provides immediate feedback on the bridge's structural health, allowing for early detection of any abnormal behavior or potential damage.

❖ Event-Triggered Assessments

In addition to routine inspections, post-tensioned bridges should be subject to assessments triggered by significant events, such as extreme weather events, earthquakes, or heavy traffic incidents. These assessments help identify any sudden damage or changes in structural behavior caused by such events.

❖ Periodic Load Testing

Periodic load testing involves applying additional load to the bridge to evaluate its response and behavior. Load tests can help identify any unusual structural responses or detect hidden damage that may not be apparent during routine inspections.

❖ Long-Term Monitoring

For post-tensioned bridges with specific vulnerability factors, long-term monitoring may be necessary. This involves monitoring the bridge's behavior and performance over an extended period to identify any gradual changes or deterioration that could lead to potential failures.

❖ Continuous Evaluation

Continuous evaluation of bridge performance through structural health monitoring techniques can aid in identifying trends and patterns over time. This approach allows for proactive maintenance and timely intervention before damage becomes severe.

In summary, the timing of damage detection in post-tensioned bridges involves a combination of regular inspections, real-time monitoring, event-triggered assessments, periodic load testing, long-term monitoring, and continuous evaluation. Early detection and timely intervention are crucial in ensuring the safety, durability, and reliability of post-tensioned bridges throughout their service life.

2.5   Cracks lead to failure

Cracks in post-tensioned bridges can indeed lead to failure if not detected and addressed promptly. The presence of cracks in a bridge indicates that the structure has experienced stress or deformation beyond its capacity, potentially compromising its structural integrity and overall safety. Here's how cracks can lead to failure in post-tensioned bridges:

Reduced Load-Carrying Capacity

Cracks in the bridge elements, such as the deck or beams, can reduce the load-carrying capacity of the structure. The cracks may weaken the material and lead to a progressive failure that cannot support the intended loads, resulting in structural collapse or significant deformation.

Corrosion Propagation

Cracks in post-tensioned bridges can provide pathways for moisture and aggressive agents to reach the embedded post-tensioning tendons or reinforcement. If these tendons or reinforcement bars are corroded due to exposure to moisture, chloride ions, or other corrosive substances, their strength can be significantly reduced, eventually leading to structural failure.

Figure 8-Corrosion (Janamian & Aguiar, 2023)

Propagation of Cracks

Cracks can propagate and spread over time due to various factors such as repeated loading, environmental effects, or inadequate repair and maintenance. As cracks widen and lengthen, the structural components become more vulnerable, potentially leading to catastrophic failure.
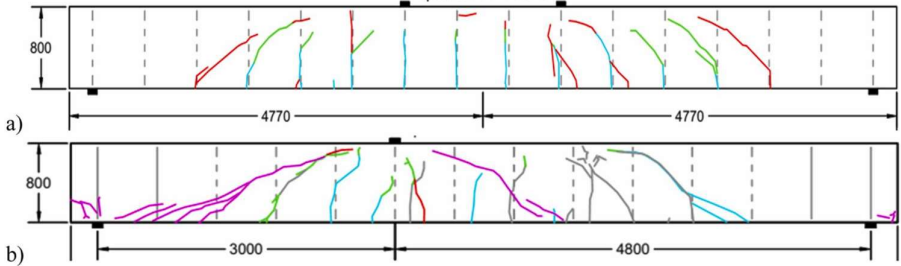

Figure 9- Propagation of Cracks (Fülöp & al., 2022)

Fatigue Failure

Repeated loading, such as heavy traffic or dynamic forces from vehicles, can cause fatigue failure in the bridge components, resulting in the initiation and propagation of cracks. Fatigue cracks can grow gradually and ultimately compromise the structural integrity of the bridge.
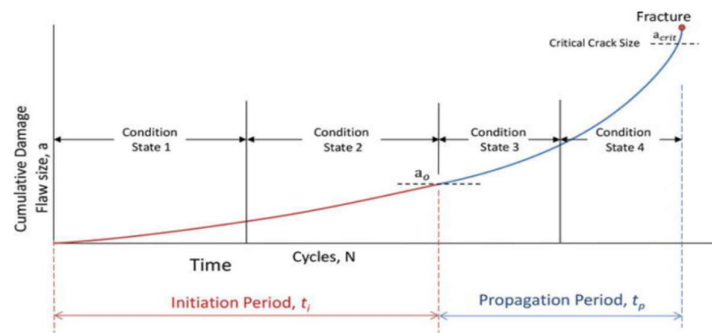
Loss of Post-Tensioning Force

Cracks in the post-tensioned ducts or anchorages can lead to the loss of post-tensioning force, reducing the pre-stress in the bridge members. This loss of pre-stress can result in excessive deflections, reduced load-carrying capacity, and potential collapse.

3 *Prestressed Concrete Bridge over Torne River(Agredo Chavez & al., 2022)*

A prestressed concrete bridge, constructed in 1963 using BBRV cables, spans three sections and extends over a total length of 134.8 meters. Due to mining activities, the bridge underwent loading from trucks weighing a combined 90 tons, both during the periods of 2012-2014 and 2019. Over time, manual observations and data collected from strain gauges and LVDTs tracked the development of cracks. These cracks typically range from 0.1 to 0.3 millimeters in width and have shown a tendency to increase in length as time passes.

In November 2020, certain strain gauges on the concrete exhibited concerning growth rates, prompting the closure of the bridge to traffic. Subsequently, new strain gauges were affixed to vertical reinforcement bars, and an evaluation ensued to determine the bridge's fatigue capacity. The findings indicated that the additional strain gauges did not register any increase in strain growth, and the bridge's fatigue capacity was deemed sufficient. Following a closure lasting five weeks, the bridge was reopened for traffic. The discussion covers aspects such as monitoring strain gauge drift and fatigue-related considerations.

Introduction :

Numerous prestressed concrete bridges worldwide have surpassed the 50-year mark, sparking inquiries into their structural health and ability to withstand loads [1]-[3]. This article focuses on a specific instance: a bridge constructed in 1963, situated over the Torne River in Autio, northern Sweden, in close proximity to the Finnish border.

Figure 11-Prestressed Concrete Bridge over Torne River at Autio built in 1963 with three spans and a total length of 134.8 m. View towards SE.

Assessment:

❖ **Heavy traffic:**

Initially, the traffic loads comprised an axle load of 140 kN, accompanied by a dynamic increment of 40%. Additionally, a distributed load of 24 kN/m was considered. A review conducted in 2011 concluded that the bridge had the capacity to support trucks with a combined load of 900 kN, traveling along the center of the bridge.
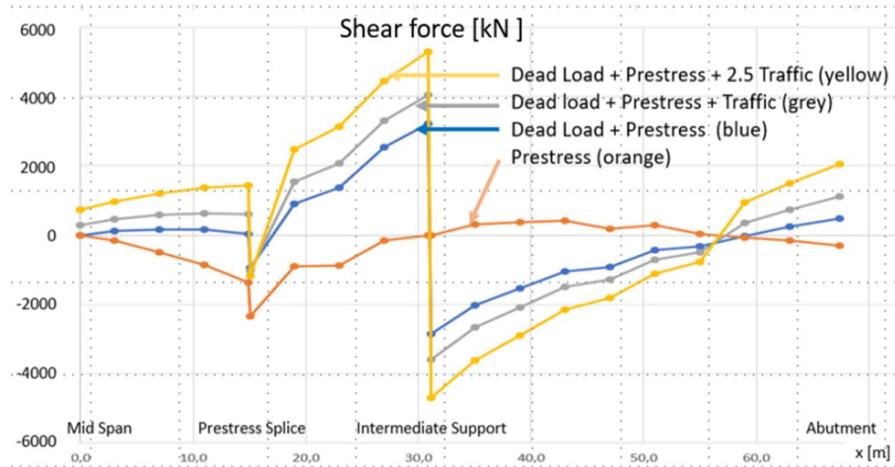
Figure 12-Shear forces according to the original design.

Subsequently, in the subsequent year, mining operations commenced nearby, leading to the passage of substantial mining trucks across the bridge. Unfortunately, the mining enterprise faced financial insolvency in 2014 owing to a decline in ore prices. In 2019, a fresh evaluation was undertaken, coinciding with the initiation of a new mining venture that involved the transit of newly introduced heavy trucks across the bridge.

❖ **Moment capacity:**

The bending moment capacity remains unaffected and without concerns. The selected models for analysis are straightforward and easily applicable. The presence of numerous prestressing cables, as depicted in Figure 3, along with their adequate lever arms, ensures sufficient capability to withstand the imposed moments.
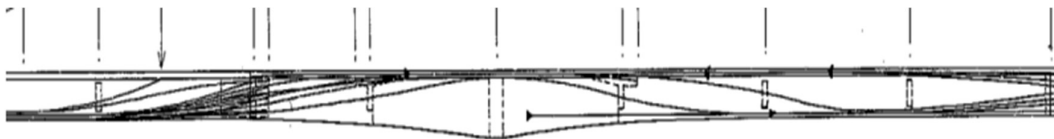
Figure 13-Prestressing reinforcement for one symmetrical half of the bridge

❖ **Shear capacity:**

The shear capacity poses more significant challenges. The original design is illustrated in Figure 2. When the traffic load is multiplied by a factor of 2.5, it results in a maximum shear force of approximately 5.5 MN. Considering the positive influence of the intermediate support, the required capacity for the beams can be reduced to about 5 MN. These applied loads yield shear stress of τ = 1.2 MPa in close proximity to

the midspan and a maximum principal stress of σI = 0.36 MPa. Given the relatively low principal concrete stresses, only a minimal shear reinforcement is necessary.

As indicated earlier, the initial design featured minimal principal stresses, which the concrete was capable of supporting. It is conceivable that the prestressing forces may have diminished over time due to factors like shrinkage, creep, and relaxation [8]. Consequently, this reduction could have elevated the principal tensile stresses to levels surpassing the concrete's tensile strength. This, in turn, might account for the extensive observed cracking, as depicted in Figure 5 and described below.
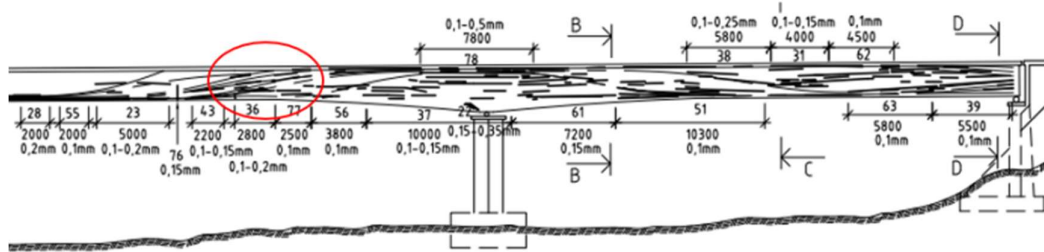
Figure 14-Cracks on the outside of the West Beam of the Autio Bridge, September 15, 2020.

If we assume a flatter crack angle more loads can be taken by the stirrups. But still there is a substantial load that must be carried by the prestressed concrete.

❖ **Cracking:**

In 2014, slender horizontal cracks emerged in the primary beams. About 20 cracks were measured, generally displaying a width ranging between 0.1 to 0.2 mm and extending over a few meters in length. With the resumption of mining activities in 2019, routine crack assessments were conducted approximately four times per annum. The majority of these cracks exhibit alignment parallel to the prestressing cables. During a September 2020 inspection (depicted in Figures 5 and 6), approximately 60 cracks were measured, showcasing widths spanning from 0.1 to 0.35 mm. Most of these displayed a width of 0.2 mm, with lengths varying from 1 to 22 meters.

The presence of these cracks appears to be a natural outcome of tensile principal concrete stresses in specific bridge sections. The combination of these stresses with thermal stresses is likely the triggering factor behind the crack formation. No signs of corrosion are evident around the cracks, and the deformations remain too minimal to suggest any stirrup yielding thus far. An ongoing investigation involves the monitoring of strains in certain stirrups to ascertain the potential existence of fatigue-related issues.

Figure 15-Crack pattern at section 77 in Figure 5 (the 1/4-point) where joints of the prestressing reinforcement are situated. There are five cracks of width 0.1 mm, but they are hard to see for the naked eye.

❖ **Monitoring:**

In 2020, measures were taken to reduce the need for frequent bridge inspections. Cracks were deliberately introduced and concrete strain gauges were attached to monitor the situation. By November 2020, some strain gauges showed concerning growth, prompting the bridge's closure due to potential factors like concrete cracks or gauge drift.

Despite thorough inspections and temperature compensation investigations, no issues were identified. Additional strain gauges were then added to reinforcement bars at different positions, which revealed no growth and insignificant stress ranges, eliminating the risk of fatigue failure. The initial strain gauges were suspected to have drifted, a known occurrence with concrete-attached gauges.

After five weeks of closure, the bridge was deemed safe for reopening. Almost a year later, in October 2021, crack measurements indicated no further crack growth, with maximum increases around 0.001 mm. Overall, the bridge's condition improved, and it was reopened after addressing the concerns.
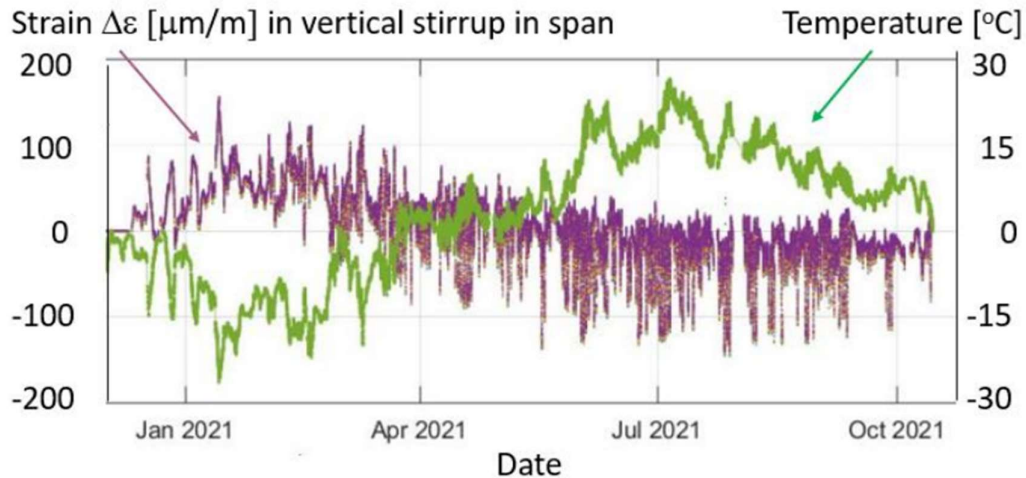
Figure 16-Strain (violet) in a vertical stirrup in midspan and Temperature (green) from Dec 2020 to October 2021. Max strain range ≈ 150 m/m. Temperature range -25 to +25 oC,

❖ **Conclusion:**

(1) The examined bridge's bending resistance and deflections appear to be satisfactory.

(2) Concerns about shear and torsion capacity due to extensive cracking have been alleviated. Evolution in design philosophy, with reduced concrete shear and tensile capacities compared to earlier standards, has contributed. The beams have minimal vertical reinforcement (φ10 c 250), relying on prestressing forces to balance shear. Factors like creep, shrinkage, relaxation (subject to further study), and thermal stresses likely contribute to the prevalent concrete cracking.

Nevertheless, the stirrups effectively withstand shear forces, showing no signs of fatigue. Monitoring indicates their potential to remain reliable for decades, possibly supported by continuous observation.

(3) We recommend employing non-destructive testing (NDT) to eliminate uncertainties about remaining prestressing force, potential corrosion, and settlement effects.

(4) In summary, the bridge is deemed safe and durable, paralleling the longevity of well-maintained bridges. It can remain in service for an extended period.

4 *CASE STUDY:*

Figure 17-Map view.

4.1 *Structure Review :*

The post-tensioned bridge, which comprises two distinct sections, each accommodating a pair of lanes and supported by individual piers, and was operationalized in 1992. Employing a cantilevered approach, the bridge consists of five spans and extends across a distance of 320 meters. This contemporary and inventive structure adopts a 'Box Segmental Girder' design, utilizing precast concrete girders with a hollow box-shaped profile, partitioned into smaller segments. This design choice guarantees efficiency in terms of structural integrity, heightened resistance to bending and shear forces, and notable torsional rigidity, rendering it exceptionally suitable for lengthy span requirements. The construction technique of the 'Box Segmental Girder' offers adaptability, reduced construction duration, and the capacity to effectively manage intricate geometries and site-specific complexities.
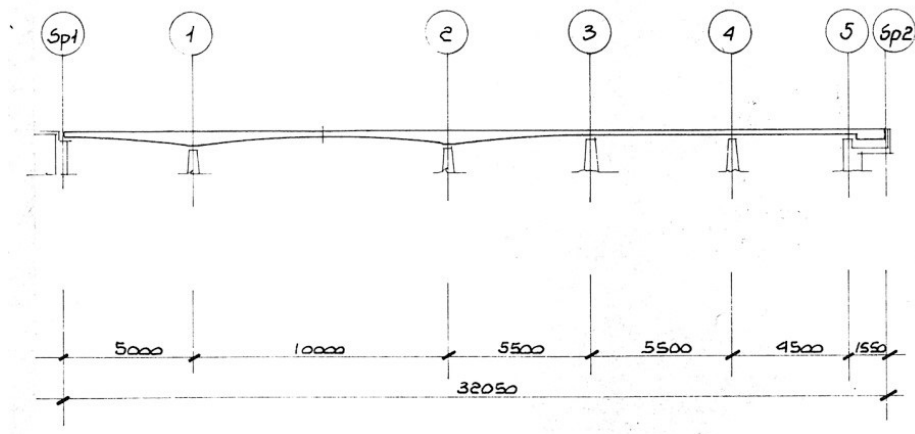
Figure 18- layout of the bridge spans.

36
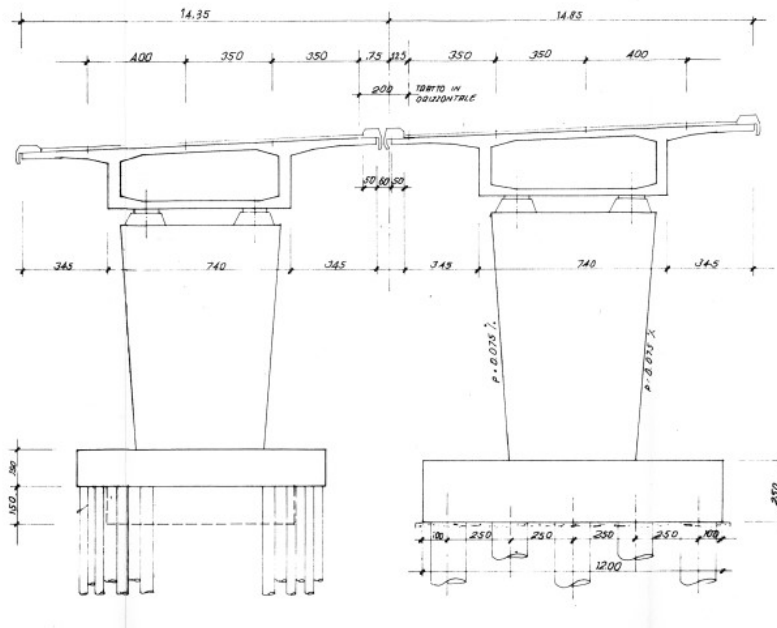
Figure 19-cross section.

❖ Pier properties:
o Foundation:
The foundations of the bridge in the plans are grouped into groups that share the same reinforcements.

> GROUP 1: 1S – 2S – 3S – 4S – 5S – 1D – 2D

The foundations for this assemblage are circular in shape and possess a uniform thickness of 3 meters. These foundations are bifurcated into two symmetrical segments: an upper ring with a 10.6-meter diameter and a lower ring with a 6.9-meter diameter. The structure is supported by a total of 136 piles, which serve as both the foundation and pile cap. Of these piles, those linked to the upper ring extend 16.5 meters, while the remaining piles measure 15 meters. To bolster these foundation components, an extensive steel reinforcement arrangement has been applied, illustrated in Figure (20). Moreover, Figure (21) presents an overview of the pile distribution that provides support for this specific style of foundation.

Figure 20-The arrangement of steel reinforcement within the foundations of group 1.
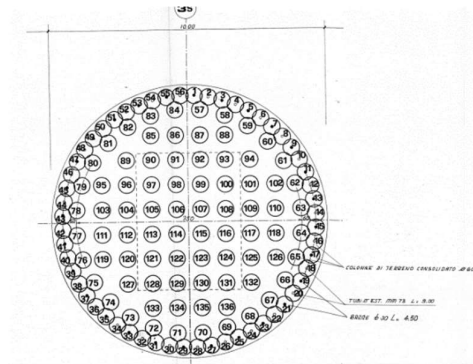
Figure 21-The arrangement of piles beneath the foundations of group 1.

➢ GROUP 2: 3D – 4D

The base of this structure features rectangular foundations, with dimensions of 8.5 meters by 12 meters, and possesses a consistent thickness of 2.5 meters. These foundations have a dual purpose, serving as both the foundation and pile cap, and are upheld by a total of 15 primary piles. Each primary pile is composed of multiple secondary piles, totaling 58 such piles. The lengths of these piles range from 10.5 to 18 meters underneath this particular foundation group. To reinforce and fortify these foundations, an elaborate arrangement of steel reinforcement has been implemented, as depicted in Figure (22).

Additionally, Figure (23) visually portrays the distribution pattern of piles that provide support to this specific foundation type.
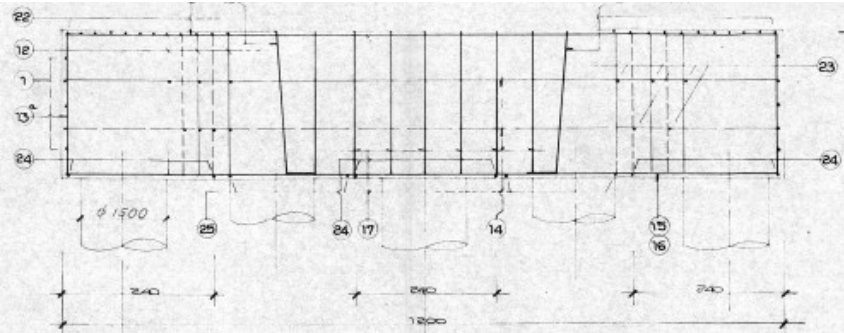
Figure 22-The configuration of steel reinforcement within the foundations of group 2.
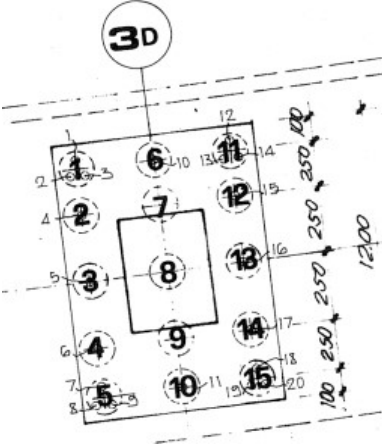
Figure 23-The arrangement of piles beneath the foundations of group 2.

➢ GROUP 3: 5D

The base of this specific group is in a rectangular shape, measuring 6 meters by 15.5 meters, with a uniform thickness of 2.5 meters. It fulfills a dual role, serving as both the foundation and the pile cap, and relies on the support of a total of 48 piles, each uniformly measuring 18 meters in length. In order to ensure robust strength and stability, an elaborate arrangement of steel reinforcement has been meticulously incorporated, as depicted in Figure (24). Additionally, Figure (25) visually presents the distribution pattern of piles, effectively highlighting their essential contribution to supporting this distinct foundation type.
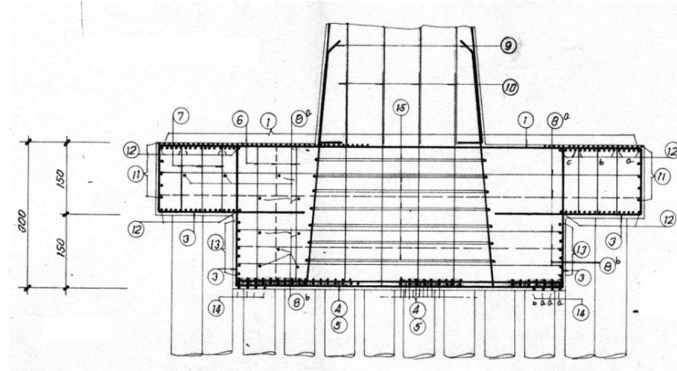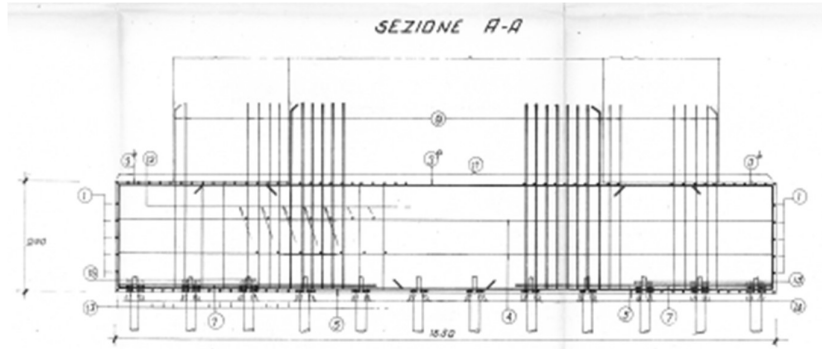
Figure 24-The design of steel reinforcement within the foundations of group 3.
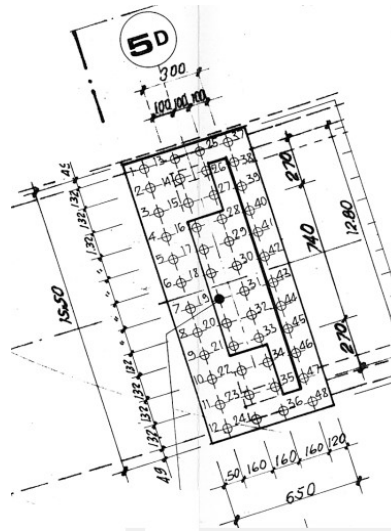
Figure 25-The arrangement of piles beneath the foundations of group 3.

o **Piles:**

Uniform reinforcement is applied to all piles, irrespective of their placement. These piles are equipped with φ24 mm longitudinal steel to provide axial strength and support for carrying loads. Furthermore, φ12 mm spiral steel is integrated to bolster lateral stability and contain the concrete within the piles. The arrangement and allocation of these steel reinforcements within the central portion of the piles are depicted in Figure (26).
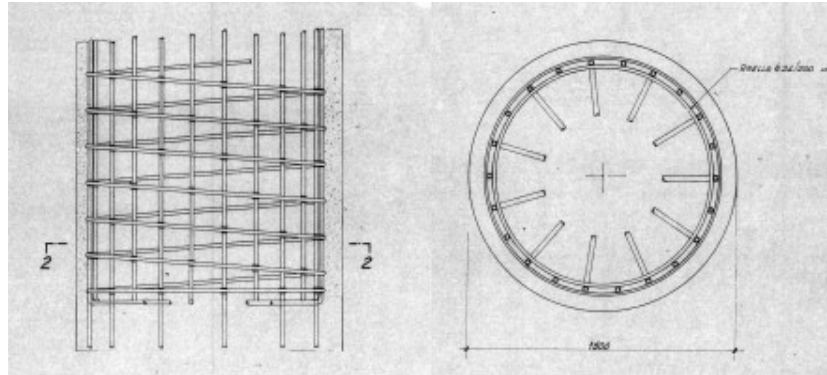
Figure 26-Arrangement of steel reinforcement within the piles.

o **Piers & Columns:**

Columns are organized into distinct groupings according to the following arrangement:

➢ Group A: 1S – 1D – 2S – 2D – 3S – 3D – 4S – 4D

Within this specific group, the columns maintain a uniform shape, yet their heights differ due to the uneven underlying terrain. The tallest column reaches approximately 10 meters in height, while the shortest measures 7.47 meters. Ensuring structural strength and stability, vertical reinforcement within the columns consists of steel bars with a diameter of ϕ 26 mm. Moreover, other steel bars, encompassing transverse and shear reinforcements, possess a diameter of ϕ 16 mm.

N: PILA	h
1S	7,471
2S	9,166
3S	10,056
4S	9,766
1D	7,674
2D	9,464
3D	9,036
4D	9,553

Figure 27-Heights of columns within Group A.

Initially, the vertical load on the structure is distributed across two pads positioned directly above the columns, as illustrated in Figure (#). Subsequently, this load is effectively transmitted to each column, facilitating their capacity to proficiently carry the vertical loads.

A comprehensive analysis of the load pads will be provided in the concluding part of this section.
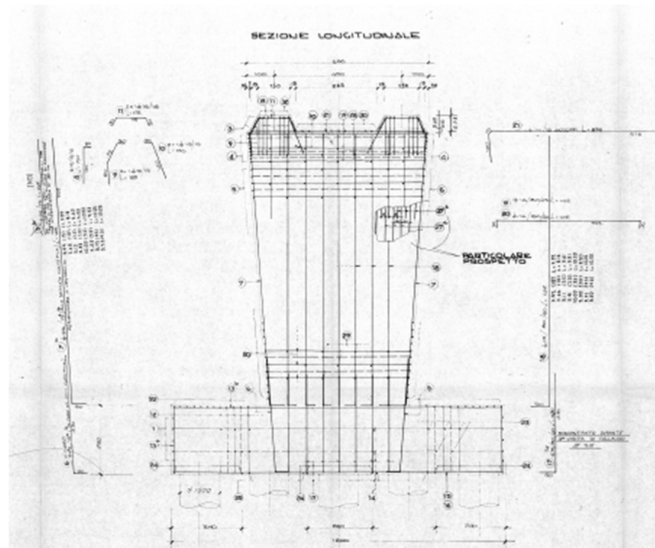
Figure 28-Cross-sectional view of columns in Group A.

➢ Group B: 5S – 5D

Within this column group, a notable characteristic distinguishes them from the rest - they function as counter-balance columns. This innovative approach incorporates a counter-balancing weight on the opposing side of the primary load, resulting in several advantages. Referred to as "counter-balance columns," these columns are strategically employed to mitigate adverse moments on the column, enhance the stability of the bridge, and enhance vibration dampening.

The reinforcement of these columns is divided into two distinct sections:

- **Column Reinforcement:** In the primary section of the column, all primary steel bars possess a diameter of ɸ 26 mm, whereas the secondary reinforcements are ɸ 16 mm in diameter.

- **Counter-Balance Side Reinforcement:** On the counter-balance side, the primary transverse reinforcements are ɸ 26 mm in diameter, while the transverse reinforcements in the opposite direction have a diameter of ɸ 20 mm. Moreover, all other secondary steel bars measure ɸ 16 mm in diameter.

To bear the vertical load of the counter-balance weight, the structure employs two pads positioned above four piles on one side and two additional pads situated above the column on the opposing side. Figure (29) illustrates the arrangement of the counterbalance column.
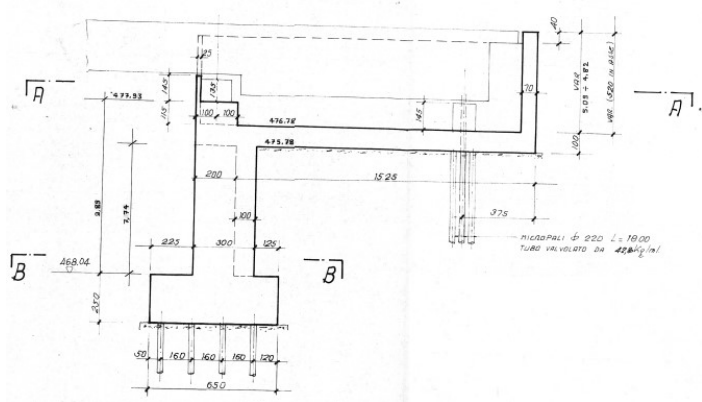
Figure 29- Counterbalance column scheme.

➤ Group C: SP1

On the other end of the bridge; susa side,
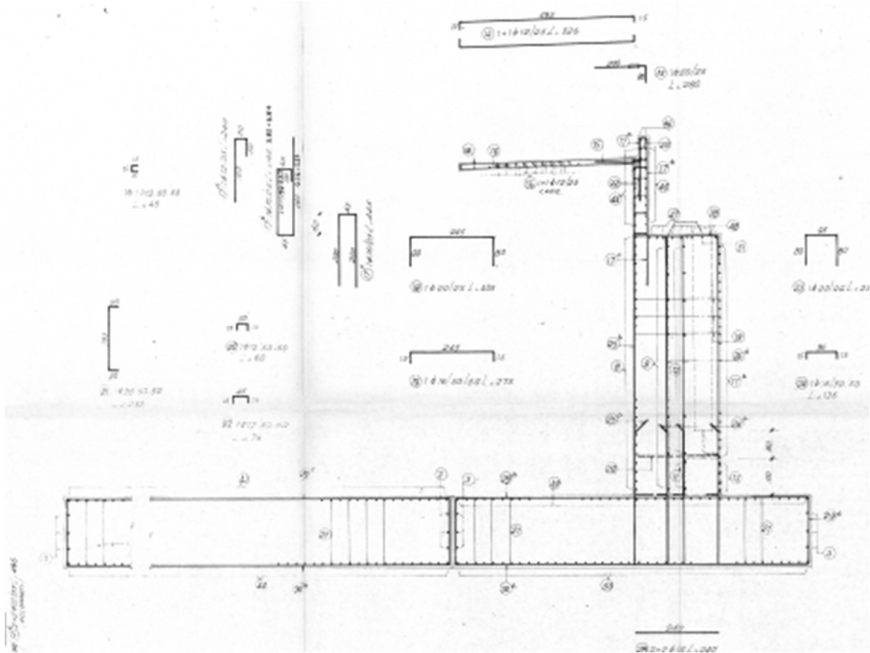
Figure 30

❖ Girders **properties**

◆ 1st span (sp1 & 1st piers):

The bridge spans a length of 50 meters and features a varying depth that ranges from 245cm to 455cm. It comprises 18 successive segments, each with varying lengths falling within the range of 180cm to 305cm. The bridge's post-tensioning system encompasses 28 upper tendons, originating from pier 1 and extending towards both sides, ultimately reaching abutment sp1 and pier 2. Furthermore, there are 6 bottom tendons that commence at abutment sp1 and extend towards the initial pier.
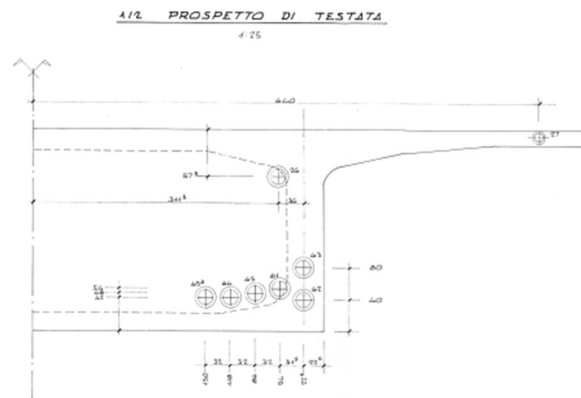
Figure 31-Cross-sectional view and arrangement of tendons at abutment sp1.

◆ 2nd span (1st & 2nd piers):

A span measuring 100 meters in length exhibits a varying depth, with measurements of 435 cm at the endpoints and 245 cm at the midspan. This span is composed of 35 sequential segments, including 5 parts at each endpoint, each spanning 260 cm, 29 parts with a length of 305 cm, and a single locking part measuring 70 cm. The post-tensioning system of the bridge comprises a total of 28 upper tendons, originating from the 1st span and extending to the midpoint of the 2nd span. Additionally, 13 lower tendons commence at the midspan between piers 1 and 2 and extend towards the piers. It's important to note that the upper tendons are replicated in the other half of the 2nd span, designated in the appendix with the identifier (B).
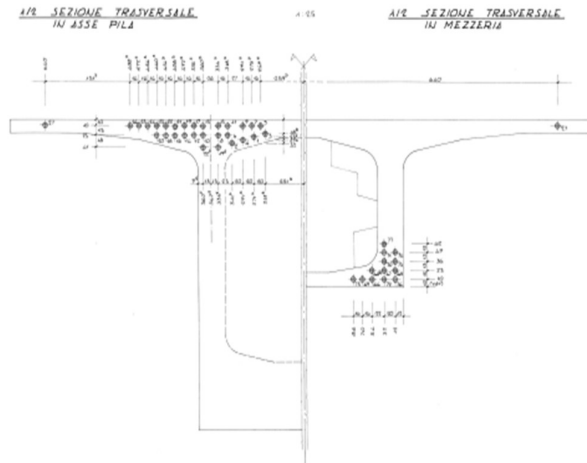
Figure 32-Cross-sectional view and arrangement of tendons between pier 1 and pier 2.

◆ 3rd span (2nd & 3rd piers):

The bridge, spanning 55 meters in length, displays a depth that varies, measuring 435cm at the left end (pier 2) and gradually tapering down to 245cm at the right end (pier 3). This bridge comprises 19 successive segments, each varying in length between 260cm and 305cm. The post-tensioning system of the bridge incorporates upper tendons, encompassing 28 tendons commencing in the latter portion of span 2 and extending into span 3. Additionally, there are an additional 12 upper tendons extending towards the midspan, originating from the 3rd pier. Furthermore, 4 lower tendons originate from the 3rd pier and traverse towards the midspan.
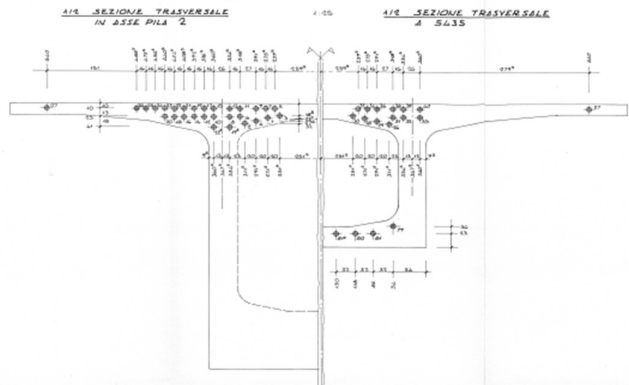
Figure 33-Cross-sectional view and arrangement of tendons between pier 2 and pier 3.

◆ 4th span (3rd & 4th pier):

The 55-meter-long bridge maintains a consistent depth of 245 cm along its entire length. Comprising 20 successive segments, the bridge includes 15 segments with an even length of 305 cm, an initial segment measuring 235 cm, and two terminal segments measuring 260 cm and 235 cm respectively. Additionally, there is a central segment acting as a lock, spanning 65 cm. The bridge's post-tensioning system features upper tendons, encompassing 12 tendons that originate in span 3 and extend into span 4. Furthermore, 14 additional upper tendons traverse towards the midspan from pier 4. Moreover, 10 lower tendons originate at the midspan between piers 3 and 4, extending towards the piers.
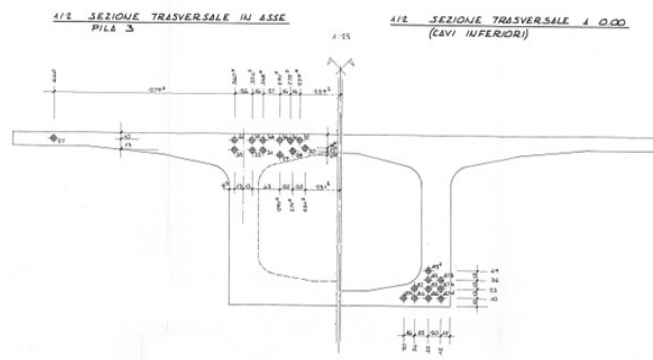
Figure 34-Cross-sectional view and arrangement of tendons between pier 3 and pier 4.

◆ 5th span (4th & 5th peer):

The bridge, spanning 45 meters in length, maintains a consistent depth of 245 cm throughout its entirety. It consists of 19 successive segments, with 15 segments uniformly measuring 305 cm in length. Additionally, there are 2 initial segments measuring 260 cm and 235 cm respectively, 5 terminal segments of 260 cm, and one final segment spanning 240 cm. The bridge incorporates a central segment serving as a lock, extending over 80 cm. The bridge's post-tensioning system incorporates upper tendons, comprising 14 tendons originating in span 4 and extending into span 5. Furthermore, 7 upper tendons start at abutment sp2 and traverse towards the midspan of span 5. Additionally, 8 lower tendons commence at the midspan between piers 4 and 5, extending towards the piers.
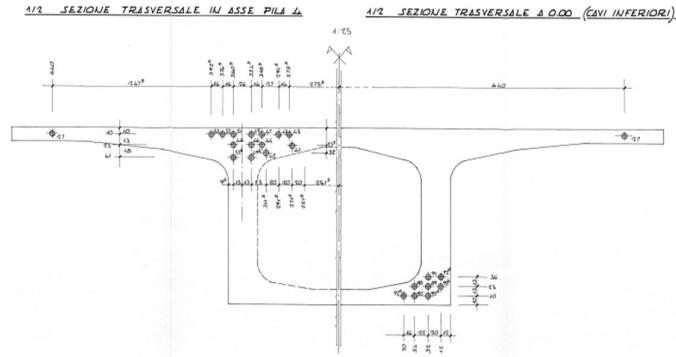
Figure 35-Cross-sectional view and arrangement of tendons between pier 4 and pier 5.

At the opposing end of pier 5, a counter-balance element measuring 15.5 meters in length is present. An important tendon, labeled as number 27, extends across all spans along the sides of the girders, as evident in all the provided sections. Furthermore, all tendons are symmetrically replicated on the opposite side of the girder, ensuring a balanced and uniform distribution of loads across the entire bridge structure. This well-thought-out design, incorporating the counter-balance feature and symmetrical duplication of tendons, significantly bolsters the bridge's stability, safety, and overall performance. This design solidifies the bridge's reputation as a dependable and efficient transportation infrastructure.

4.2   Cracks Review :

As a critical part of this maintenance, a comprehensive inspection was conducted on the Bridge to evaluate its condition and assess any existing cracks. This inspection aimed to meticulously examine the bridge's surface, measure the width of each crack, and gather essential data that would provide insights into the structural health and performance of the bridge.

The inspection process was carried out with precision and meticulous attention to detail, employing state-of-the-art techniques and equipment. This effort was not only essential for ensuring the longevity of the bridge but also for safeguarding the safety of the individuals who rely on it for their daily commutes and transportation needs.
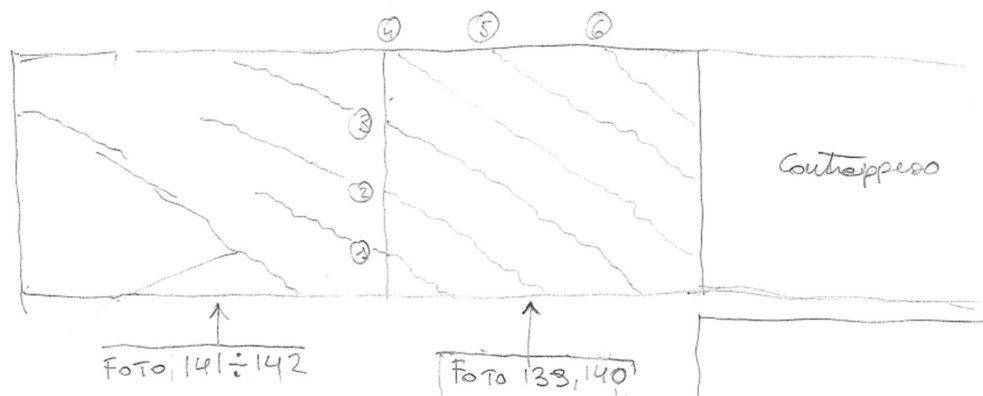
Figure 36- Cracks path.

Photo 141   *Photo 142*

Photo number	Crack number	Width (mm)
124	1	0.2
125	2	0.8
126	3	0.9
127	4	0.5
128	5	0.8
129	6	0.7

Table 2

Photo 124

Photo 125

Photo 126
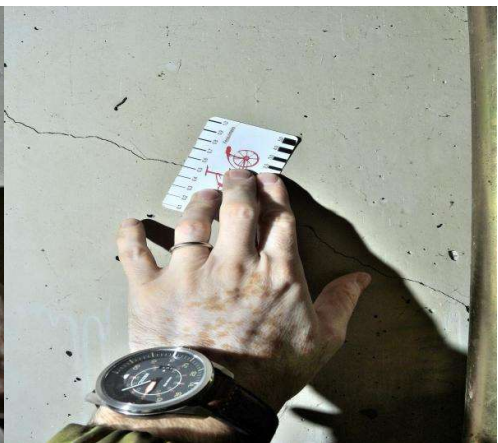
Photo 127

Photo 128   *Photo 129*
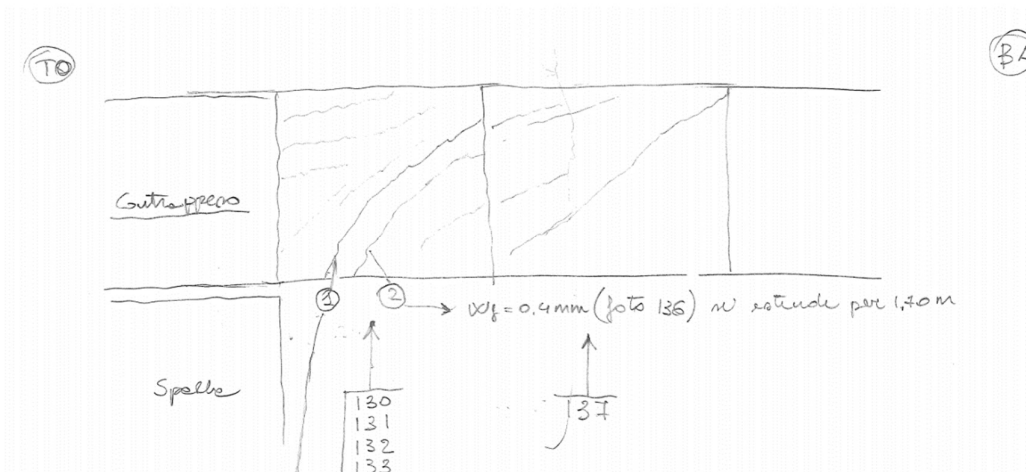
Figure 37-Cracks Path.

Based on the information provided, Crack Number 1 exhibits a width of 1.2 mm over a length of 1.35 meters. The representation of this crack is captured in Photo 135.

Photo 135

Crack Number 2 is characterized by a width of 0.4 mm occurring at intervals of every 1.7 meters. This crack is visually represented in Photo 136. Understanding the presence and dimensions of cracks, such as Crack Number 2, is essential for evaluating the structural condition of concrete elements.
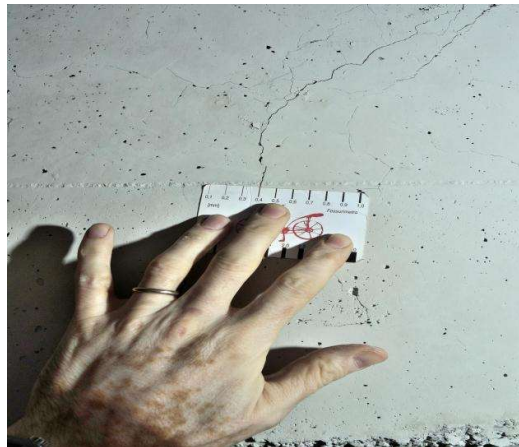
Photo 136

Photo number	Crack number	Width (mm)
135	1	1.2
136	2	0.4

Table 3- Crack width.

In the below images we can see thee section , and detailed reinforcement where the crack is happening .
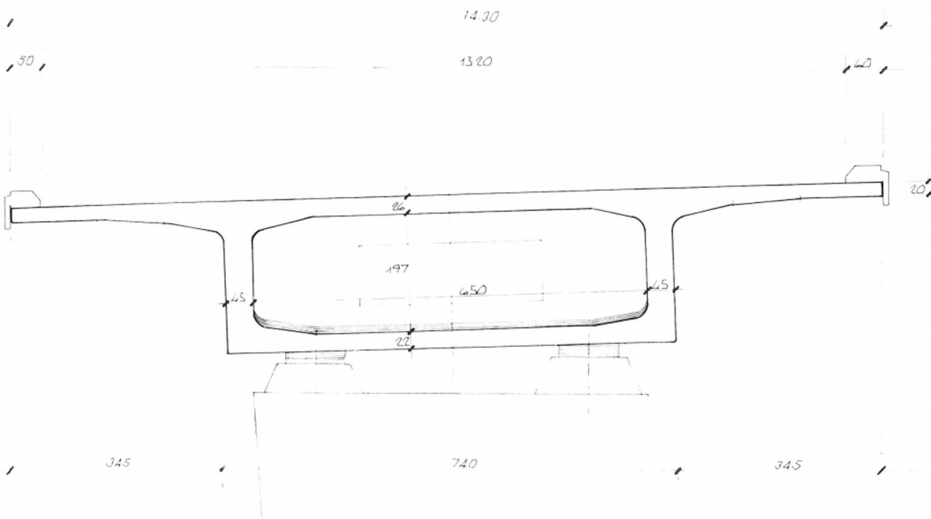
Figure 38- Box girder section.
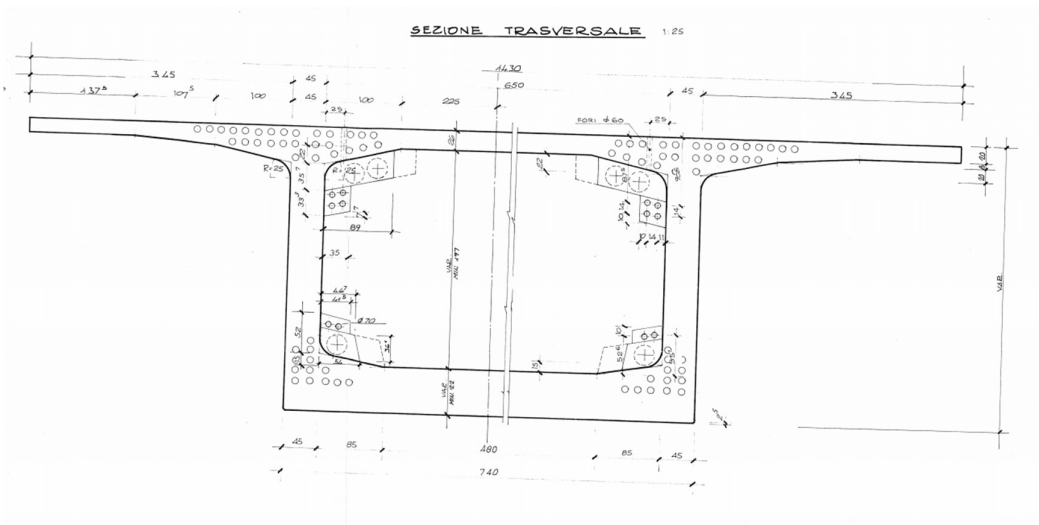
Figure 39- Box girder section.

PROSPETTO 1:25

N.B. PREVEDERE FORI
PER SCARICO ACQUE
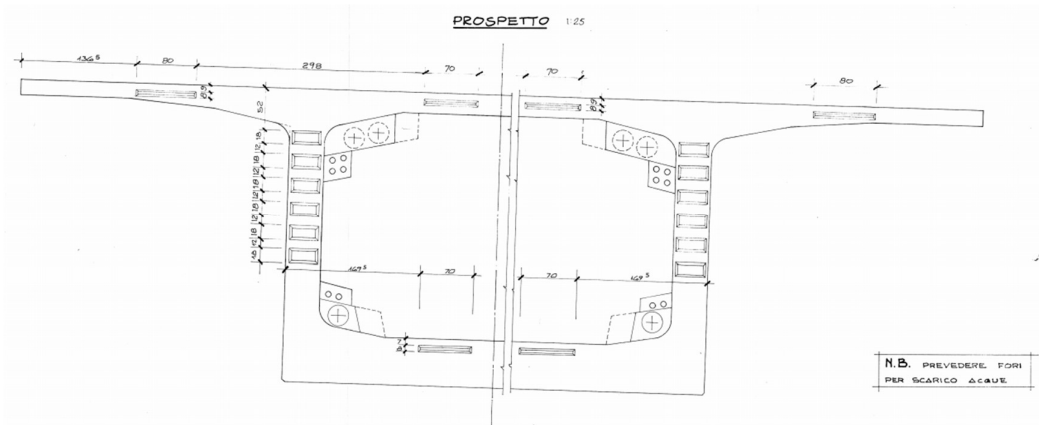
Figure 40- Box girder section.

❖ **Detailed cross-section**

Reinforcement distribution:
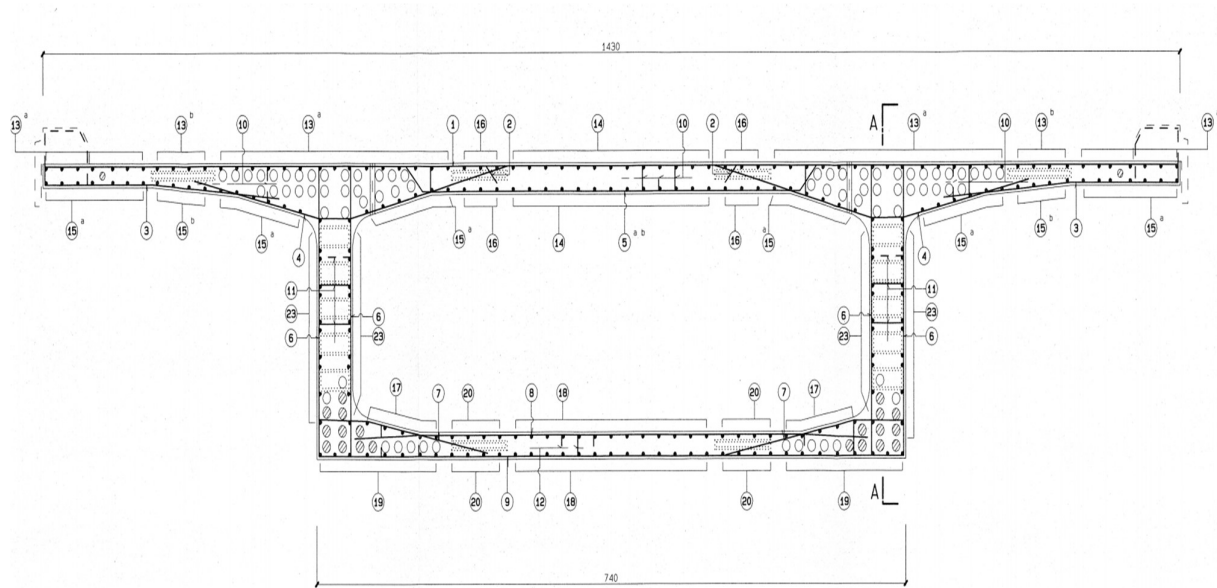
Figure 41- Girder section.
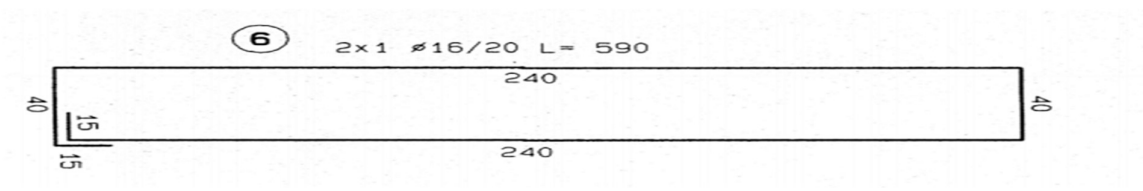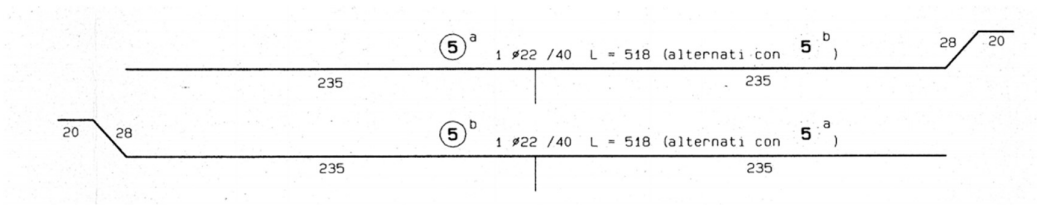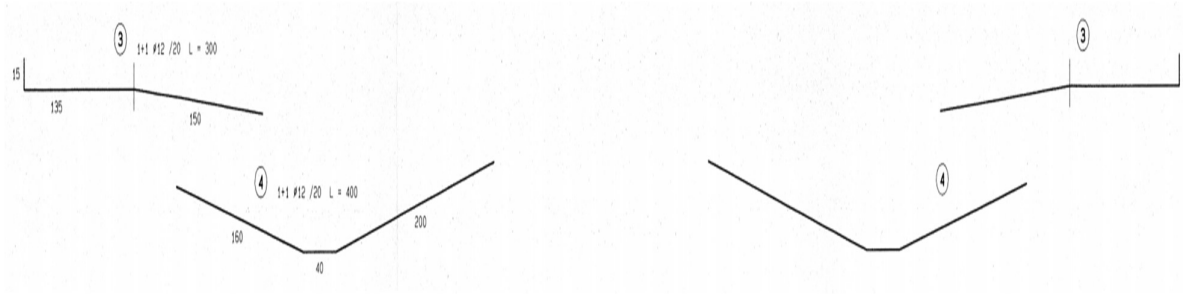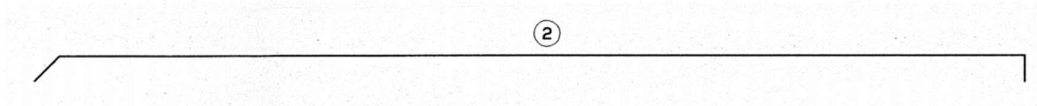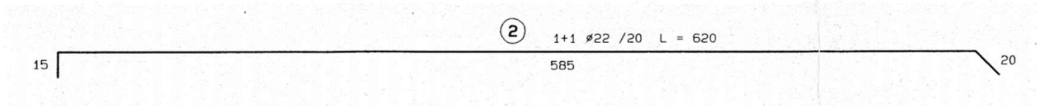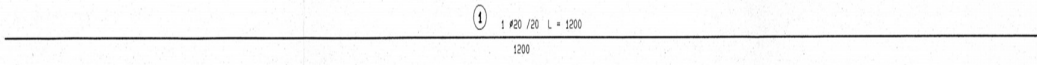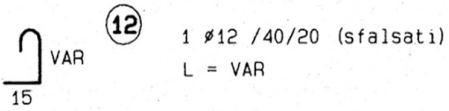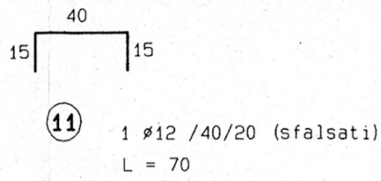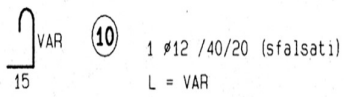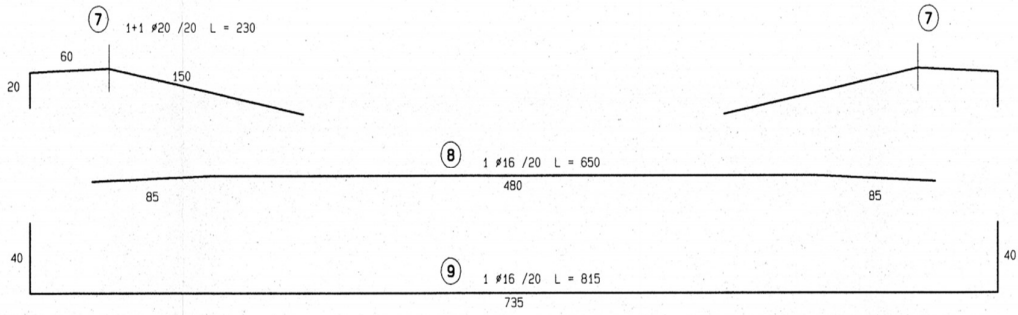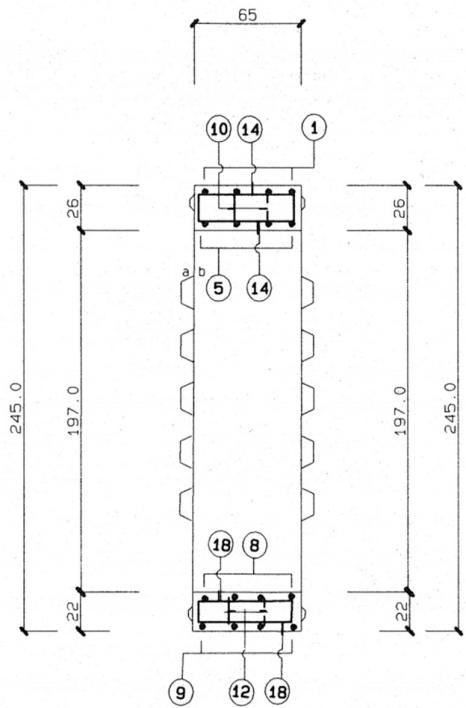
① 1 ⌀20 /20 L = 1200

1200

② 1+1 ⌀22 /20 L = 620

15   585   20

②

③ 1+1 ⌀12 /20 L = 300

15

135   150

④ 1+1 ⌀12 /20 L = 400

160   200

40

③

④

⑤ᵃ 1 ⌀22 /40 L = 518 (alternati con 5ᵇ)

235   235   28 20

20 28

⑤ᵇ 1 ⌀22 /40 L = 518 (alternati con 5ᵃ)

235   235

⑥ 2x1 ⌀16/20 L= 590

240

40   40

15

15

240

54

⑦ 1+1 Ø20 /20 L = 230

60

20

150

⑦

⑧ 1 Ø16 /20 L = 650

85   480   85

40   40

⑨ 1 Ø16 /20 L = 815

735

VAR ⑩ 1 Ø12 /40/20 (sfalsati)
                  L = VAR
15

40

15 ⌐   ⌐ 15

⑪ 1 Ø12 /40/20 (sfalsati)
                L = 70

VAR ⑫ 1 Ø12 /40/20 (sfalsati)
                  L = VAR
15

55

longitudinal section:

particular section A - A:
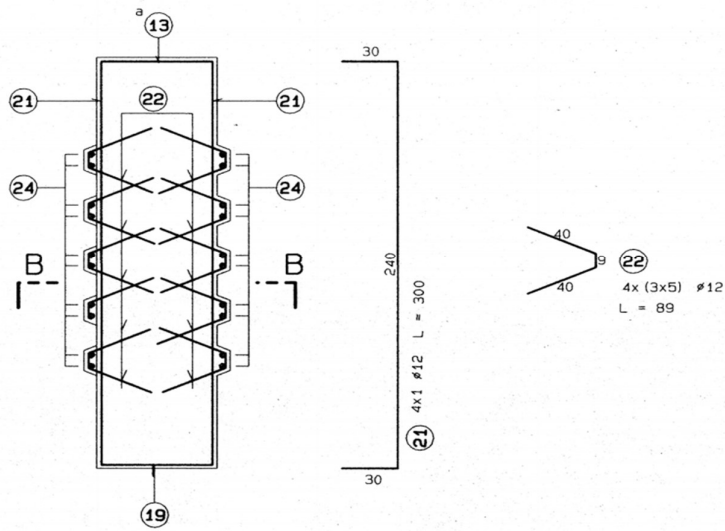
horizontal section B - B:

57
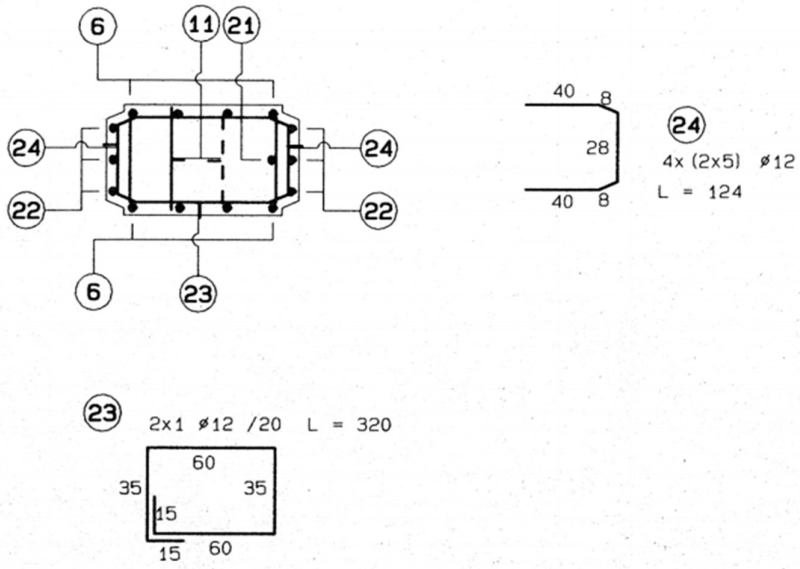
4.3 Material used:

◆ REINFORCEMENT STEEL (C.A):
For carpentry steel, the density value is assumed to be γ_s = 7850 daN/m^3

- The characteristic yielding strength f_{syk}= 4500 daN/cm^2

- The characteristic failure strength f_{suk}= 5400 daN/cm^2

SLU condition f_{syd}= 4500 /(1,15) = 3913 daN/cm^2

SLE condition f_{syd}= = 4500/(1,25) = 3600 daN/cm^2

◆ CONCRETE:
Listed below are the principal mechanical attributes and characteristics established in accordance with the reference standard (NTC2018). In the case of concrete, the following density per unit volume is adopted: γ_{cls} = 2500 daN/m^3

Concrete class C50/60

Characteristic cylinder compressive strength	f_{ck} (MPa)	50
Characteristic cube compressive strength	$f_{ck,cube}$ (MPa)	60
Mean cylinder compressive strength	f_{cm} (MPa)	58
Mean tensile strength	f_{ctm} (MPa)	4.07
Elastic modulus	E_{cm} (MPa)	37278
Design compressive strength (for αcc=1.00)	f_{cd} (MPa)	33.33
Design compressive strength (for αcc=0.85)	f_{cd} (MPa)	28.33

Design tensile strength (for αct=1.00)	f_{ctd} (MPa)	1.90
Minimum longitudinal tension reinforcement ratio	ρ_{min} (%)	0.212
Minimum shear reinforcement ratio	$\rho_{w,min}$ (%)	0.113

Table 4

4.4   *Introduction to Traffic Load Consideration:*

Bridges experience both permanent and transient loads, with live loads being primarily dynamic. These dynamic loads, stemming from sources like traffic, rolling stock, and locomotives, have both vertical and horizontal components. When analyzing these loads, engineers often use static analysis, incorporating dynamic amplification factors as needed to consider the dynamic effects. Importantly, live loads on bridges are not stationary; they can shift to critical positions as traffic moves across the span, in contrast to permanent loads with fixed positions as per code regulations.

Therefore, it becomes necessary to conduct a Moving Load Analysis, which is essentially a form of Static Load Analysis aimed at identifying the most critical load effects among the various potential positions along the bridge. This analysis relies on methods like Influence Line analysis or influence surface analysis to determine these critical positions.
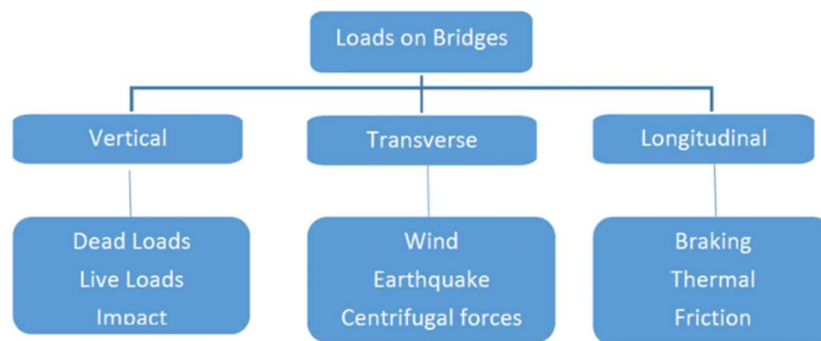
Figure 42-Nature of Loading on Bridges.

LOAD ANALYSIS :

In this chapter, our objective is to provide a comprehensive explanation of the loads employed and the various loading scenarios to be applied in accordance with both Eurocode and the Italian technical standards.

DEAD LOAD - Deck

self-weight which is variable in accordance with the shape of the section the specific weight of the section is 25kn/m3.

TRAFFIC LOADS

The EN 1991-2 standard outlines traffic load models for the structural design of road bridges, footbridges, and railway bridges. When designing new bridges, EN 1991-2 is intended to be used alongside the EN 1990-1999 Eurocodes for direct application, serving as a design guideline. However, it should be compared with national reference guides.

EN 1991-2 precisely defines the imposed loads, including models and representative values, associated with road traffic, pedestrian activities, and rail traffic. These specifications encompass dynamic effects, as well as actions such as centrifugal forces, braking, acceleration, and accidental design actions when relevant.

Under normal usage conditions (excluding accidental situations), traffic and pedestrian loads should be regarded as variable actions. The diverse representative values include:

➤ characteristic values.
➤ frequent values.
➤ quasi-permanent values.

The table outlines the fundamental criteria used as a basis for fine-tuning the primary load models applicable to both road bridges and footbridges.

Traffic Load Models	Characteristic values	Frequent values	Quasi-permanent values
Road bridges			
LM1 (4.3.2)	1000 year return period (or probability of exceedance of 5% in 50 years) for traffic on the main roads in Europe (α factors equal to 1, see 4.3.2).	1 week return period for traffic on the main roads in Europe (α factors equal to 1, see 4.3.2).	Calibration in accordance with definition given in EN 1990.
LM2 (4.3.3)	1000 year return period (or probability of exceedance of 5% in 50 years) for traffic on the main roads in Europe (β factor equal to 1, see 4.3.3).	1 week return period for traffic on the main roads in Europe (β factor equal to 1, see 4.3.3).	Not relevant
LM3 (4.3.4)	Set of nominal values. Basic values defined in annex A are derived from a synthesis based on various national regulations.	Not relevant	Not relevant
LM4 (4.3.5)	Nominal value deemed to represent the effects of a crowd. Defined with reference to existing national standards.	Not relevant	Not relevant
Footbridges			
Uniformly distributed load (5.3.2.1)	Nominal value deemed to represent the effects of a crowd. Defined with reference to existing national standards.	Equivalent static force calibrated on the basis of 2 pedestrians/m^2 (in the absence of particular dynamic behaviour). It can be considered, for footbridges in urban areas, as a load of 1 week return period.	Calibration in accordance with definition given in EN 1990.
Concentrated load (5.3.2.2)	Nominal value. Defined with reference to existing national standards.	Not relevant	Not relevant
Service vehicle (5.3.2.3)	Nominal value. As specified or given in 5.6.3.	Not relevant	Not relevant

Table 5-Load model characteristics. Source: EN 1991-2.

The design of this bridge relies on Load Model 1, LM1, which accounts for concentrated and evenly distributed loads. This model effectively encompasses the impact of traffic from both cars and trucks, making it suitable for both general and localized structural assessments.

To elaborate on the nature of these dynamic loads, they originate from various forms of road traffic, including regular vehicles, trucks, lorries, and specialized industrial transport vehicles. It encompasses all potential variations in pedestrian and transient loads that can occur over the bridge's lifespan.

The carriageway area, denoted by its width "w," should be viewed as a unified space bounded by curbs or any internal road constraints. National regulations will outline the specific width requirements based on the road's classification and type. The determination of notional lane count should adhere to the principles outlined in the following table.

Carriageway width w	Number of notional lanes	Width of a notional lane w_l	Width of the remaining area
$w < 5,4$ m	$n_1 = 1$	3 m	$w - 3$ m
$5,4$ m $\leq w < 6$ m	$n_1 = 2$	$\dfrac{w}{2}$	0
6 m $\leq w$	$n_1 = Int\left(\dfrac{w}{3}\right)$	3 m	$w - 3 \times n_1$
NOTE For example, for a carriageway width equal to 11m, $n_1 = Int\left(\dfrac{w}{3}\right) = 3$, and the width of the remaining area is 11 - 3×3 = 2m.			

Table 6-Classification of notional lanes. Source EN1991.

4.4.1 LOAD MODEL 1, LM1

Traffic loads are assessed using LM1 because it provides comprehensive data for both general and localized assessments and verification. Essentially, this model comprises two distinct subsystems:

➢ TS, tandem system. It is a double axle concentrated loads, each having a certain load declared form the rules.
➢ UDL, uniformed distributed loads, that has weight per square metre along the notional lane. The UDL should be applied only in the unfavourable position along the deck.

The following scheme represents the variable loads applied for traffic loads.

Position	TS [kN]	UDL [kN/m²]
Notional lane 1	300	9,00
Notional lane 2	200	2,50
Notional lane 3	100	2,50
Remaining area	-	2,50

Table 7-Traffic loads.

As previously outlined in the variable load description, the calculation approach involves longitudinal primary beams with lateral overhangs. These beams are periodically subjected to distributed loads, which have a fixed width of 3.00 m or can vary depending on their intended use. These loads are strategically positioned to achieve and identify the most extreme loading scenarios on either the outer beams or the central beam.

DISPERSAL OF CONCENTRATED LOADS:

As previously discussed, assessing concentrated loads on continuous elements presents challenges since they do not conform to De Saint Venant's theory. Therefore, they should be treated as unique loads that require specialized scrutiny for evaluation.

The distribution beneath the concentrated load's footprint should be assessed with a spreading pattern that extends at a 1:1 ratio to the depth, sloping at a 45° angle. The image provides a concise illustration of the localized impact.
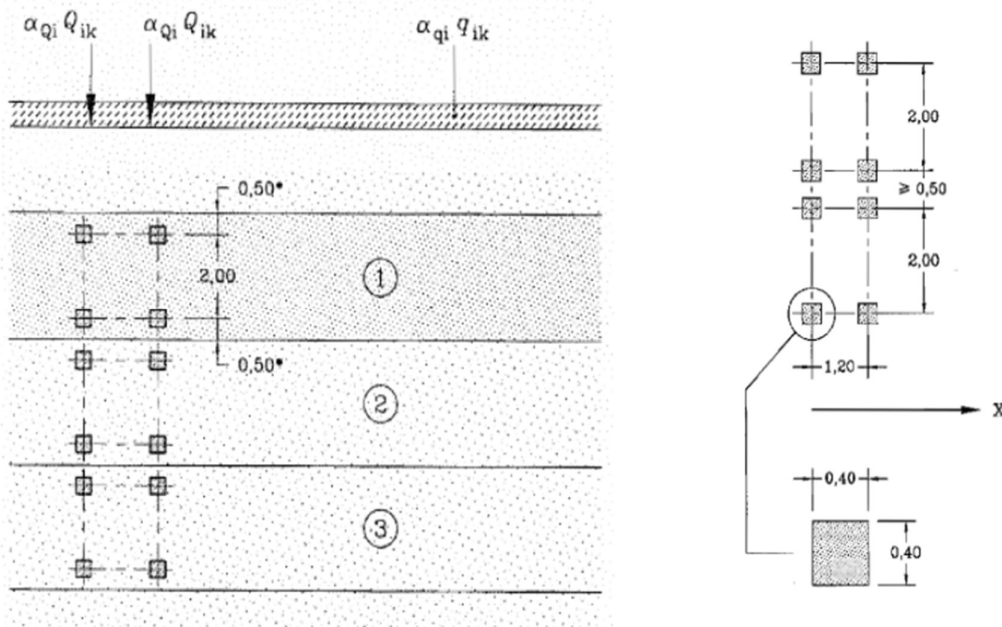
Figure 43-Geometrical condition of LM1. Source EN1991.
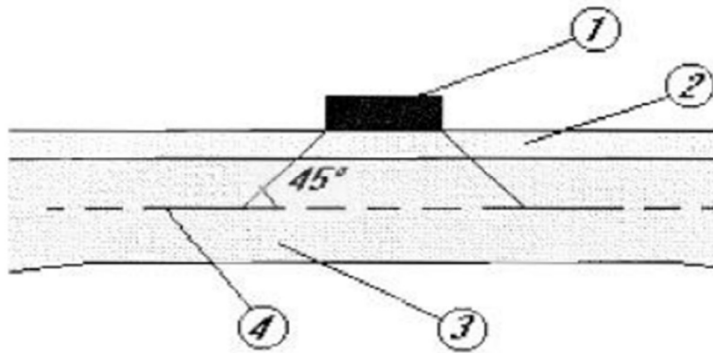
Figure 44-Representation of load distribution through the pavement. Source EN 1991.

Where,

- ➢ 1, wheel contact pressure.
- ➢ 2, Pavement layer.
- ➢ 3, concrete slab
- ➢ 4, middle surface of concrete slab.

4.4.2 HORIZONTAL FORCES – BRAKING, ACCELERATION & CENTRIFUGAL

When conducting checks for horizontal forces induced by mobile elements, it's essential to consider the characteristic component of these forces.

A braking force, denoted as Q_{lk}, should be treated as a longitudinal force exerted at the surface level of the roadway. Its characteristic magnitude is capped at 900 kN for the entire bridge width. Importantly, this force calculation is derived as a proportion of the maximum vertical loads from LM1 on notional lane 1. The formula is as follows:

$$Q_{lk} = 0.6(2Q_{1k}) + 0.1(q_{1k}.w.L)$$

Where,

- ➢ w, notional lane width.
- ➢ L, bridge length.
- ➢ Q_{lk}, UDL corresponded.

64

It is important to bear in mind that when evaluating this force, it should be placed along the axis of the notional lane.

Acceleration forces should be considered with an equal magnitude to the braking force but in the opposite direction.

Centrifugal force. It is an action acting at the carriageway level, both transversely and in radial direction due to its vector components. In this specific case, it will not be included in the calculation of dynamic actions, since it is dependent on the radius of curvature of the road path.

4.4.3   WIND EFFECTS

The wind load is computed following the guidelines outlined in chapter §3.3 of NTC2018, which align with the Eurocode EN 1991-1-4. This load is analogous to a stationary horizontal force, oriented perpendicular to the bridge's axis and projected onto the vertical plane of the relevant surfaces. In situations where the bridge is loaded with vehicles, the exposed surface area expands due to their presence. This expanded area can be likened to a continuous rectangular wall positioned 3 meters above the road surface.(Trasporti, 20018)

a)   REFERENCE BASE VELOCITY

The fundamental reference speed, denoted as "V_b " is determined by calculating the mean velocity over a 10-minute period at a height of 10 meters above the ground. This measurement is conducted on a flat and uniform terrain classified under exposure category II (as per Table 3.3.II of NTC2018) and is associated with a return period of 50 years. The table provided below presents the reference values essential for assessing the base velocity.

Zona	Descrizione	$v_{b,0}$ [m/s]	a_0 [m]	k_s
1	Valle d'Aosta, Piemonte, Lombardia, Trentino Alto Adige, Veneto, Friuli Venezia Giulia (con l'eccezione della provincia di Trieste)	25	1000	0,40
2	Emilia Romagna	25	750	0,45
3	Toscana, Marche, Umbria, Lazio, Abruzzo, Molise, Puglia, Campania, Basilicata, Calabria (esclusa la provincia di Reggio Calabria)	27	500	0,37
4	Sicilia e provincia di Reggio Calabria	28	500	0,36
5	Sardegna (zona a oriente della retta congiungente Capo Teulada con l'Isola di Maddalena)	28	750	0,40
6	Sardegna (zona a occidente della retta congiungente Capo Teulada con l'Isola di Maddalena)	28	500	0,36
7	Liguria	28	1000	0,54
8	Provincia di Trieste	30	1500	0,50
9	Isole (con l'eccezione di Sicilia e Sardegna) e mare aperto	31	500	0,32

Table 8-provides an explanation of the Italian zone, with its source being NTC 2018.
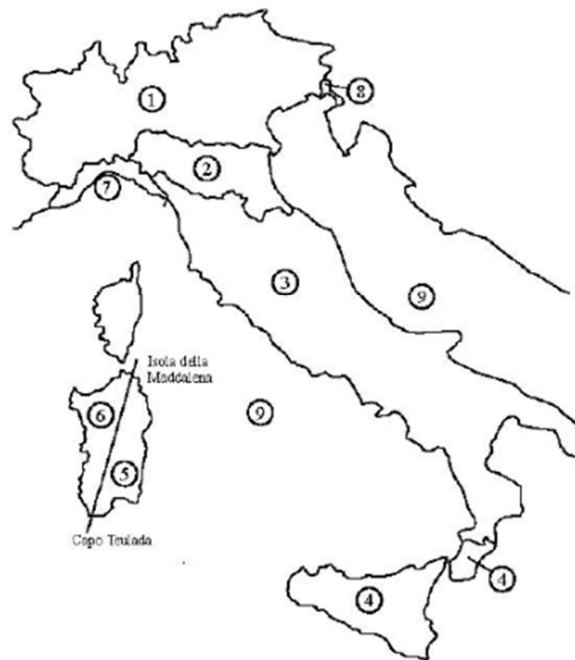
Figure 45-Geographical subdivision of base reference velocity. Source NTC2018.

As outlined in the technical regulations:

$$v_b = v_{b0} \cdot c_a$$

$$\left[\begin{array}{l} c_a = 1, \quad a_s \le a_0 \\[2mm] c_a = 1 + k_s \left(\dfrac{a_s}{a_0} - 1 \right), \quad a_0 < a_s < 1500m \end{array} \right.$$

In this case, we obtain:

$$v_b = 27 \cdot 1 = 27 \text{ m/s}$$

b) **WIND KINETIC PRESSURE:**

To compute the reference kinetic pressure, denoted as "q_b" (in N/m2), we have employed the formula provided in chapter §3.3.4 of NTC18.

$$q_b = \frac{1}{2} p \cdot v_r^2$$

Where "r" represents the standard air density, which is equivalent to 1.25 kg/m3, and "v_r" signifies the reference velocity.

c) **EXPOSURE COEFFICIENT**

As outlined in the Italian technical regulations, the exposure coefficient is directly influenced by the elevation above ground level and the characteristics of the local terrain topography. This coefficient is determined using factors associated with tabulated values found in NTC18, including exposure category, ground roughness, and proximity to the sea. Calculating this coefficient based on these parameters is a straightforward process.

In accordance to the rule, the coefficient is evaluated as:

$$C_e(z) = k_r^2 \cdot c_t \cdot \ln\left(\frac{z}{z_0}\right) \cdot \left[7 + c_t \cdot \ln\left(\frac{z}{z_0}\right)\right] \qquad z \geq z_0$$

$$C_e(z) = C_e(z_{min}) \qquad z < z_{min}$$

Categoria di esposizione del sito	K_r	z_0 [m]	z_{min} [m]
I	0,17	0,01	2
II	0,19	0,05	4
III	0,20	0,10	5
IV	0,22	0,30	8
V	0,23	0,70	12

Table 9-Exposure coefficients related to each case. Source NTC 2018.

ZONE 1,2,3,4,5

	2 km	10 km	30 km	500m	750m	
A	- -	IV	IV	V	V	V
B	- -	III	III	IV	IV	IV
C	- -	*	III	III	IV	IV
D	I	II	II	II	III	**

* Categoria II in zona 1,2,3,4
Categoria III in zona 5

** Categoria III in zona 2,3,4,5
Categoria IV in zona 1

ZONA 9

A	- -	I
B	- -	I
C	- -	I
D	I	I

ZONA 6

	2 km	10 km	30 km	500m	
A	- -	III	IV	V	V
B	- -	II	III	IV	IV
C	- -	II	III	III	IV
D	I	I	II	II	III

ZONE 7,8

	1.5 km	0.5 km	
A	- -	- -	IV
B	- -	- -	IV
C	- -	- -	III
D	I	II	*

* Categoria II in zona 8
Categoria III in zona 7
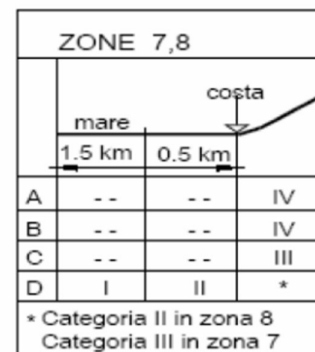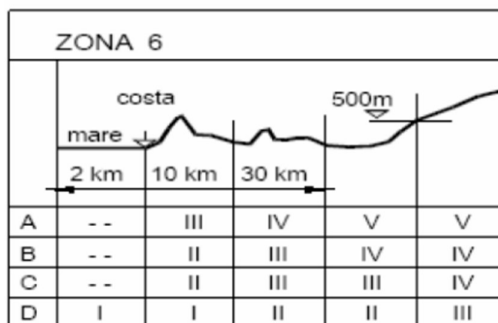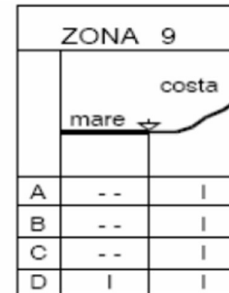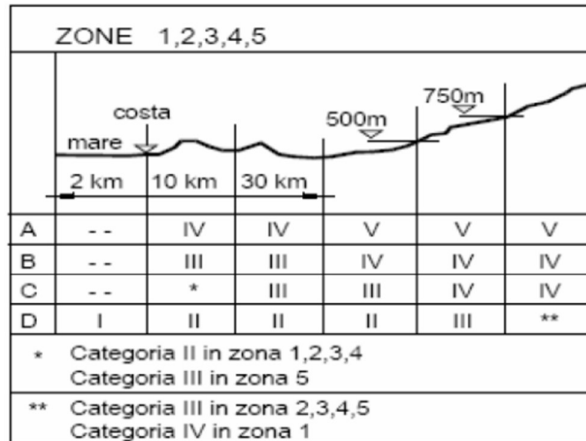
Figure 46-Definition of the class of exposure related to the case. Source NTC2018.

Following this, a concise overview will be provided for all the values utilized in the computation.

BASE REFERENCE VELOCITY		
a_s	238	m
a_0	500	m
k_s	0,37	-
$v_{b,0}$	27	m/s
c_a	1	
v_b	27	m/s
REFERENCE VELOCITY		
c_r	1,0392386	
T_R	100	anni
v_r	28,059441	m/s
KINETIC BASE PRESSURE		
q_r	492,08265	N/m2
EXPOSURE CLASS PARAMETERS		
Exposure class		IV
Roughness ground		B
k_r	0,22	m
z_0	0,3	m
z_{min}	8	-
c_t	1	-
c_d	1	-
φ	1	-
c_p	1,4	-
d	3900	mm
h	2500	mm
d/h	1,56	-
μ	0,2	-

Table 10-Reference Parameters of wind.

ELEVETION			EXPOSURE COEFFICCIENT		
Z_1	9,7	m	c_e	1,7625321	-
Z_2	10,1	m	c_e	1,7898992	-
Z_3	13,1	m	c_e	1,9698166	-

LATERAL PRESSURE			DOWNWIND			DOWNWIND		
p_1	1214,2361	N/m2	p_1	242,84721	N/m2	p_1	48,569443	N/m2
p_2	1233,0897	N/m2	p_2	246,61793	N/m2	p_2	49,323586	N/m2
p_3	1357,0376	N/m2	p_3	271,40752	N/m2	p_3	54,281504	N/m2

Table 11-Geometrical values and pressures.

4.4.4 TEMPERATURE EFFECT

Fluctuations in outdoor temperature, solar radiation, and convection, which occur on a daily and seasonal basis, result in temperature variations within the individual structural components. The intensity of thermal effects is typically affected by numerous factors, including the climate at the site, the degree of exposure, the total mass of the structure, and the potential inclusion of insulating non-structural elements.

> ### UNIFORM THERMAL VARIATION

The constant temperature component is naturally influenced by the highest and lowest temperatures reached by the bridge. According to the European standard EN 1991-1-5, which addresses the temperature fluctuations of a composite deck, specifically of type 2, the upper and lower values can be specified as follows:

$$T_{e,max} = T_{max} + 4 = 41,5 + 4 = 44,5 \,°C.$$

$$T_{e,min} = T_{min} + 4 = -4.1 + 4 = 0,1 \,°C.$$

4.4.5 LOAD COMBINATION CRITERIONS

In this section, we will examine the safety assessment standards for the forces outlined in the preceding chapter and how they are applied to structural models.(Trasporti, 2008)

The Ultimate Limit States are listed below:

- ✓ Structural stability loss or imbalance.
- ✓ Excessive displacements or deformations.
- ✓ Attainment of the utmost resistance capacity in structural components, connections, and foundations.
- ✓ Achievement of the highest resistance capacity of the entire structure.
- ✓ Activation of collapse mechanisms within the soil.

- ✓ Failure of membranes and connections due to fatigue.
- ✓ Failure of membranes and connections due to other time-related factors.
- ✓ Instability in structural components or the entire structure.

The main Exercise Limit States are listed below:

- ✓ Specific harm like extensive concrete cracking, which has the potential to diminish the structure's longevity, functionality, or aesthetics.
- ✓ Movements and deformations that have the potential to restrict the utility, efficiency, or visual appeal of the construction.
- ✓ Displacements and deformations that might hinder the effectiveness and visual aspects of non-structural elements, equipment, and machinery.
- ✓ Vibrations that have the potential to undermine the structure's usability.
- ✓ Fatigue-related harm that could jeopardize longevity.
- ✓ Material corrosion and/or substantial degradation due to the environmental conditions.

Regarding the crack assessment, the verification is performed following the guidelines established in Circular dated 21 January 2009, number 7, titled "Instructions for the implementation of the Technical Standards for construction updates." These guidelines are referenced in the Ministerial Decree of 17 January 2018.

The characteristic width for crack verification, denoted as "W_k" can be computed using the following formula:

$$W_k = 1{,}7\varepsilon_{sm}.\Delta_{sm}$$

Where, ε_{sm} is the average unit deformation of reinforcement.

$$\varepsilon_{sm} = \frac{[\sigma_s - k_t\left(\frac{f_{ctm}}{\rho_{eff}}\right)(1 + \alpha_e \rho_{eff})]}{E_s}$$

σ_s, is the tension stress in the reinforcement considering the cracked section.

α_e, is the ratio E_s/E_{cm}.

ρ_{eff} , is the ratio $A_s/A_{c,eff}$. $A_{c,eff}$ is the effective concrete are without reinforcement.

k_t,is a partial coefficient linked to the load duration.

Δ_{sm} , is the average distance between the cracks.

To facilitate the inspection of crack distances or the maximum spacing between bars in a convenient and indirect manner, NTC18 provides two significant tables for quickly assessing reinforcement. These tables are depicted below.

Tensione nell'acciaio	Diametro massimo ϕ delle barre (mm)		
σ_s [MPa]	$w_3 = 0{,}4$ mm	$w_2 = 0{,}3$ mm	$w_1 = 0{,}2$ mm
160	40	32	25
200	32	25	16
240	20	16	12
280	16	12	8
320	12	10	6
360	10	8	-

Table 12-Maximum diameter of bar to crack control. NTC2018.

Tensione nell'acciaio	Spaziatura massima s delle barre (mm)		
σ_s [MPa]	$w_3 = 0{,}4$ mm	$w_2 = 0{,}3$ mm	$w_1 = 0{,}2$ mm
160	300	300	200
200	300	250	150
240	250	200	100
280	200	150	50
320	150	100	-
360	100	50	-

Table 13-Maximum span between bars to crack control. NTC2018.

LOAD COMBINATIONS

Chapter 5 of the NTC addresses general principles and technical guidelines for designing and constructing road bridges and railways. Specifically, for road bridges, it not only outlines the primary geometric attributes but also specifies various potential loading agents and designates load patterns that correspond to the variable actions imposed by traffic. The load patterns designated for both road and rail applications in static and fatigue assessments are typically in alignment with the schemes defined in UNI EN 1991-2.

The term "bridges" encompasses all types of structures that, based on their distinct functions, are commonly referred to by specific designations, including viaducts, underpasses, overpasses, elevated roadways, and so forth.

In the context of this regulation, the width of the bridge's roadway refers to the measurement taken perpendicular to the axis of the road.

When it comes to hydraulic compatibility, it is imperative to precisely establish the return period for flooding, for instance, with a T_R of 200 years. Providing a detailed description and specification in the hydraulic and hydrogeological report is of utmost significance in elucidating all the factors that impact the viability of this undertaking.

The factors to be taken into account during the design of road bridges encompass: permanent forces; external deformations and strains imposed; dynamic forces stemming from traffic; varying forces (including temperature fluctuations, hydrodynamic pressures, wind, snow, and impacts on railings); passive constraints; impacts on vehicle safety barriers; seismic forces; and accidental forces.

Load Combinations. The load combinations for verification must be established to guarantee safety in line with the guidelines specified in Chapter §2. To ascertain the characteristic values of actions associated with traffic, it is typically advisable to consider combinations involving the following elements, as outlined in the table below: (NTC2018)

| Gruppo di azioni | Carichi sulla superficie carrabile | | | | | Carichi su marciapiedi e piste ciclabili non sormontabili |
| | Carichi verticali | | | Carichi orizzontali | | Carichi verticali |
	Modello principale (schemi di carico 1, 2, 3, 4 e 6)	Veicoli speciali	Folla (Schema di carico 5)	Frenatura	Forza centrifuga	Carico uniformemente distribuito
1	Valore caratteristico					Schema di carico 5 con valore di combinazione 2,5KN/m²
2a	Valore frequente			Valore caratteristico		
2b	Valore frequente				Valore caratteristico	
3 (*)						Schema di carico 5 con valore caratteristico 5,0KN/m²
4 (**)			Schema di carico 5 con valore caratteristico 5,0KN/m²			Schema di carico 5 con valore caratteristico 5,0KN/m²
5 (***)	Da definirsi per il singolo progetto	Valore caratteristico o nominale				

(*) Ponti pedonali
(**) Da considerare solo se richiesto dal particolare progetto (ad es. ponti in zona urbana)
(***) Da considerare solo se si considerano veicoli speciali

Table 14-Characteristics action values due traffic loads.

The table furnishes the partial safety factor values to be employed in the analysis for calculating the effects during the assessment of ultimate limit states. The significance of the symbols is as follows:

γ_{G1} , partial coefficient for dead load

γ_{G2} , partial coefficient for not structural loads.

γ_{Q} , partial coefficient for traffic loads.

γ_{Qi}, partial factor for variable loads.

		Coefficiente	EQU[1]	A1	A2
Azioni permanenti g_1 e g_3	favorevoli	γ_{G1} e γ_{G3}	0,90	1,00	1,00
	sfavorevoli		1,10	1,35	1,00
Azioni permanenti non strutturali [2] g_2	favorevoli	γ_{G2}	0,00	0,00	0,00
	sfavorevoli		1,50	1,50	1,30
Azioni variabili da traffico	favorevoli	γ_Q	0,00	0,00	0,00
	sfavorevoli		1,35	1,35	1,15
Azioni variabili	favorevoli	γ_{Qi}	0,00	0,00	0,00
	sfavorevoli		1,50	1,50	1,30
Distorsioni e presollecitazioni di progetto	favorevoli	$\gamma_{\varepsilon 1}$	0,90	1,00	1,00
	sfavorevoli		1,00[3]	1,00[4]	1,00
Ritiro e viscosità, Cedimenti vincolari	favorevoli	$\gamma_{\varepsilon 2}, \gamma_{\varepsilon 3}, \gamma_{\varepsilon 4}$	0,00	0,00	0,00
	sfavorevoli		1,20	1,20	1,00

Table 15-Partial coefficient for ULS load combinations.

Azioni	Gruppo di azioni (Tab. 5.1.IV)	Coefficiente ψ_0 di combi-nazione	Coefficiente ψ_1 (valori frequenti)	Coefficiente ψ_2 (valori quasi permanenti)
Azioni da traffico	Schema 1 (carichi tandem)	0,75	0,75	0,0
	Schemi 1, 5 e 6 (carichi distribuiti)	0,40	0,40	0,0
	Schemi 3 e 4 (carichi concentrati)	0,40	0,40	0,0
	Schema 2	0,0	0,75	0,0
	2	0,0	0,0	0,0
	3	0,0	0,0	0,0
	4 (folla)	--	0,75	0,0
	5	0,0	0,0	0,0
Vento	a ponte scarico SLU e SLE	0,6	0,2	0,0
	in esecuzione	0,8	0,0	0,0
	a ponte carico SLU e SLE	0,6	0,0	0,0
Neve	SLU e SLE	0,0	0,0	0,0
	in esecuzione	0,8	0,6	0,5
Temperatura	SLU e SLE	0,6	0,6	0,5

Table 16-Partial combination coefficients for variable loads.

> **ULS AND SLS LOAD COMBINATIONS**

In accordance with the §2.5.3 of Ministerial Decree 27/01/18, the following combinations of actions are defined for the purpose of checking the limit states:

1) Fundamental combination, generally used for ultimate limit states (U.L.S.)

$$\gamma_{G1} \cdot G_1 + \gamma_{G2} \cdot G_2 + \gamma_{Q1} \cdot Q_{k1} + \gamma_{Q2} \cdot \psi_{02} \cdot Q_{k2} + \gamma_{Q3} \cdot \psi_{03} \cdot Q_{k3} + \cdots$$

2) Characteristic combination (rare), generally used for irreversible limit states (S.L.S.)

$$G_1 + G_2 + Q_{k1} + \psi_{02} \cdot Q_{k2} + \psi_{03} \cdot Q_{k3} + \cdots$$

3) Frequent combination, generally used for reversible operating limit states (S.L.S.)

$$G_1 + G_2 + \Psi_{11} \cdot Q_{k1} + \Psi_{22} \cdot Q_{k2} + \Psi_{23} \cdot Q_{k3} + \cdots$$

4) quasi-permanent combination, generally used for long-term effects (S.L.S.)

$$G_1 + G_2 + \Psi_{21} \cdot Q_{k1} \quad \Psi_{22} \cdot Q_{k2} + \Psi_{23} \cdot Q_{k3} + \cdots$$

5) Exceptional combination, used for the final limit states related to exceptional actions A.

$$G_1 + G_2 + A_D + \Psi_{21} \cdot Q_{k1} \quad \Psi_{22} \cdot Q_{k2} + \Psi_{23} \cdot Q_{k3} \quad \cdots$$

The conventional understanding of a structure's nominal VN (design life) is the projected duration, in years, for which the structure is expected to sustain particular performance standards, provided it undergoes required maintenance. Table 2.4 in the 2018 National Building Code (NTC 2018) outlines the minimum VN values for different construction types, which can also inform the consideration of time-related forces.

	TIPI DI COSTRUZIONI	Valori minimi di V_N (anni)
1	Costruzioni temporanee e provvisorie	10
2	Costruzioni con livelli di prestazioni ordinari	50
3	Costruzioni con livelli di prestazioni elevati	100

Figure 47- Minimum values of the Nominal Design Life (VN) for different types of constructions (NTC 2018)

According to the NTC 2018 (National Building Code), the checking of serviceability limit states (SLS) such as cracking conditions is important because it ensures that a structure performs acceptably under everyday service conditions throughout its intended lifespan. While ultimate limit states (ULS) focus on preventing collapse or failure of the structure, serviceability limit states address aspects like durability, comfort, and aesthetics, which are crucial for the structure's long-term usability and maintenance. By checking for cracking conditions under SLS, engineers can ensure that the structure remains functional and visually appealing while also maintaining its structural integrity.

5   FEM MODELING:

5.1   Concrete elements and constitutive relations

In this segment, the diverse material models in ABAQUS for simulating concrete are discussed. Modeling materials in computer programs pose a challenge due to their nonlinear properties, demanding comprehensive data about material behavior. ABAQUS offers options like linear, nonlinear, isotropic, and anisotropic material models. To simulate the deformational behavior of reinforced concrete, a plain concrete cracking model is employed in conjunction with rebar beam elements. Various concrete constitutive models designed to account for cracking include the smeared crack concrete model, brittle cracking model, and concrete damaged plasticity model, each elaborated upon below.

Concrete exhibits either brittle or ductile behavior depending on the type of loading it undergoes. In the brittle mode, micro-cracks merge to form macro-cracks, representing areas of deformation, particularly under tension and tension-compression stress states. This behavior is associated with shear and mixed mode fracture mechanisms. Micro-cracks in the brittle mode propagate uniformly and rapidly, leading to localized deformation. On the contrary, ductile behavior occurs under compression stress states and involves distributed micro-cracking mechanisms. It showcases significant plastic deformation before fracture, with cracks spreading only as stress increases. Upon reaching the ultimate strain, concrete enters a degradation phase (softening behavior), continuing to deform until eventual failure.

The smeared crack model in ABAQUS is designed to depict behavior under low confining pressures. Initially, when subjected to compression loading, concrete exhibits an elastic response, with the unload/reload behavior being elastic as well. As stress increases, the material's behavior is dominated by cracking, leading to inelastic straining. This process continues until the ultimate stress is reached, and the material undergoes softening. The presence of cracks has an impact on both the stiffness and stress within the concrete. There are two approaches to smear cracking: the fixed crack model and the rotating crack model. In fixed crack models, crack direction and plane are constrained, assuming that all crack strain components are connected to all components of the crack traction vector. Rotating crack models propose that the crack plane rotates, remaining perpendicular to the current direction of the maximum principal strain.(Yosef Nezhad Arya, 2015)
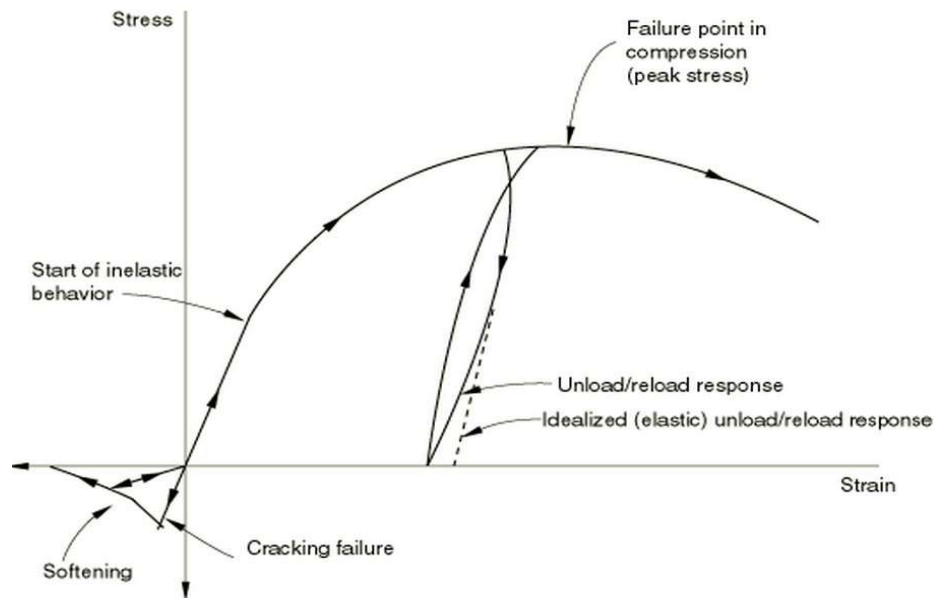
Figure 48-Uniaxial response of concrete.

The brittle cracking model in ABAQUS assumes a linear elastic compression behavior and is recommended for situations where concrete is prone to tensile cracking. Smeared cracking with fixed and orthogonal directions is presumed in this material model. The user specifies the number of cracks in a given point, and brittle failure occurs once this predefined number is reached.

On the other hand, the damaged plasticity model for concrete in ABAQUS, derived from the Drucker-Prager strength hypothesis, is a plasticity-based model tailored for analyzing concrete structures subjected to monotonic, cyclic, and/or dynamic loading. Plasticity entails irreversible deformation when all loads are removed, while damage is characterized by a reduction in elastic constants. To accurately represent the nonlinear behavior of concrete, plasticity must be combined with damage. Under low confining pressures and uniaxial compression (and tension), concrete exhibits brittle behavior. This behavior transitions when sufficient confining pressure prevents crack propagation, and when the material is exposed to multiaxial compressive stresses, resulting in increased ductility and compressive strength, as illustrated in Figure #. The damaged plasticity model incorporates the yield function of Lubliner et al. to depict the varying evolution of strength under tension and compression.
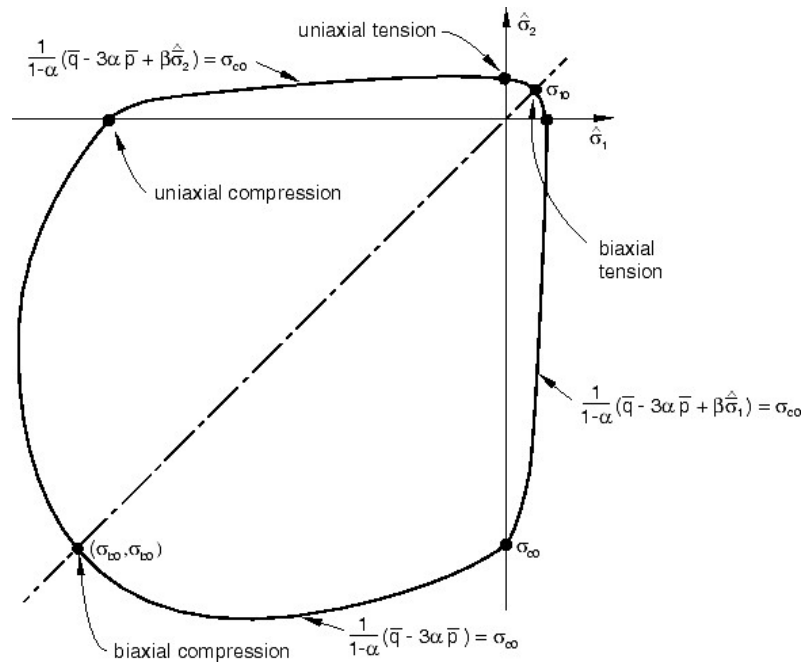
Figure 49-Yield surface for plane strain conditions at biaxial stress states.(Yosef Nezhad Arya, 2015)

The plastic potential's inclination at high confining pressures is quantified by the dilation angle, which characterizes concrete's response to various stresses. Lower values result in brittle behavior, while higher values yield ductile behavior. For normal grade concrete experiencing biaxial stress states in both tension and compression, the dilation angle should be selected within the range of 25° to 40

The plastic potential eccentricity influences the shape of the plan's meridian in stress space and is determined by the ratio of tensile strength to compressive strength, expressed as fb0/fc0. This ratio signifies the relationship between strength in the uniaxial state and strength in the biaxial state.

The stress-strain curve for concrete, outlined in section 3.1.5 of Eurocode 2 (refer to the Figure), comprises a linear-elastic region up to the point of initial yield, followed by a plastic phase involving stress hardening and subsequent strain softening.

In the absence of test results to ascertain the stress-strain curve for concrete, utilizing the mean compressive strength f_{cm} allows for curve plotting. Additional parameters required to determine the points on the graph include:

$$E_{cm} = 22(0,1f_{cm})^{0,3}$$

$$\varepsilon_{c1} = 0,7(f_{cm})^{0,31}$$

$$\varepsilon_{cu} = 3,5\%_0$$

Where:

f_{cm} is in [MPa]

E_{cm} is the longitudinal modulus of elasticity in [GPa]

ε_{c1} is strain at average compressive strength.

ε_{cu} is the ultimate strain.

If the concrete grade is higher than C50/60, the following formulas can be used:

$$\varepsilon_{c1} = 0,0014[2 - \exp(-0,024f_{cm}) - \exp(-0,140f_{cm})]$$

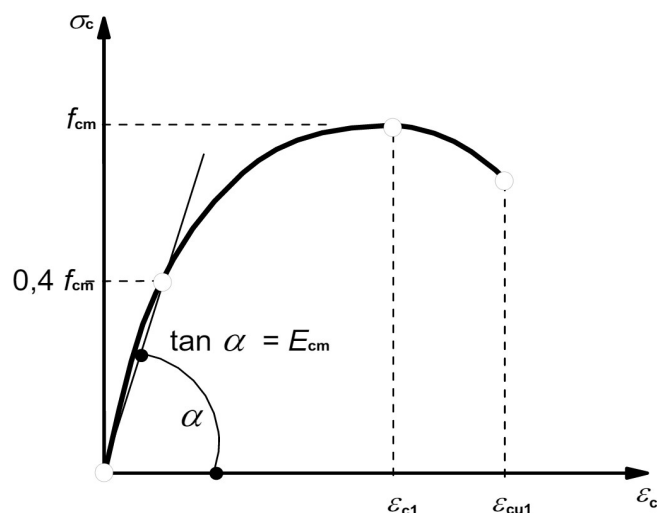$$\varepsilon_{cu} = 0,004 - 0,0011[1 - \exp(-0,0215f_{cm})]$$

Figure 50-Stress-strain curve of concrete .

Once the graph is plotted, variables characterizing compressive behavior can be derived. The inelastic (crushing) strain sin, resulting from the emergence of micro-cracks merging into macro-cracks, is determined by subtracting the elastic compressive component sel from the total strain sc (refer to Figure #). ABAQUS then converts the inelastic strain to plastic strain spl.

$$\varepsilon_c^{in} = \varepsilon_c - \varepsilon_{0c}^{el}$$

$$\varepsilon_c^{el} = \varepsilon_c^{in} \left(\frac{d_c}{1-d_c}\right)\left(\frac{\sigma_c}{E_0}\right)$$

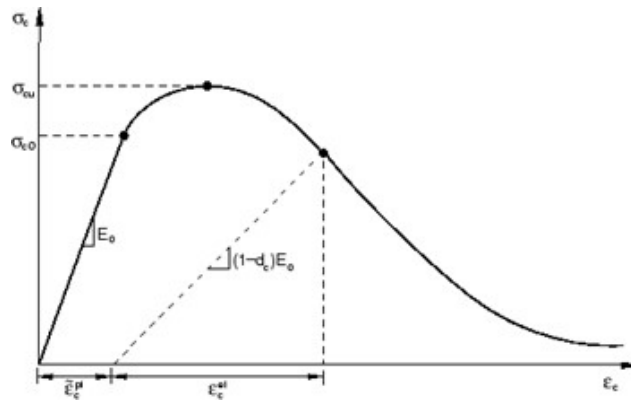$$\varepsilon_{0c}^{el} = \frac{\sigma_c}{E_0}$$

Figure 51-Illustration of inelastic stress-strain curve.

To model the post-failure behavior, tension stiffening is implemented through the application of a fracture energy cracking criterion (refer to Figure #). The stress-strain curve for tension is determined using a bilinear crack opening curve.

$$f_{ctm} = 0.3(f_{ck})^{\frac{2}{3}} \qquad\qquad\qquad \text{concrete grades} \leq C50$$
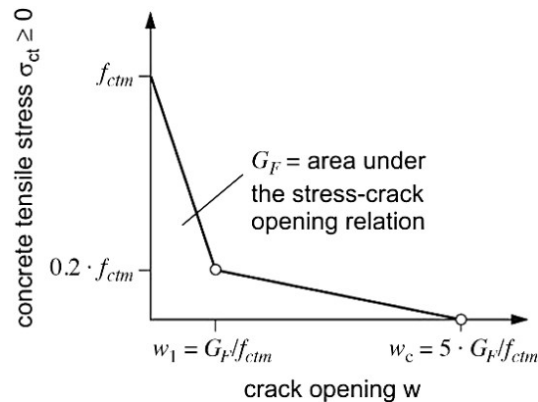
$$f_{ctm} = f_{ck} + 8$$

Figure 52-Stress-crack opening relation for uniaxial tension.(Code, 2010)

To depict material behavior accurately, it is essential to define damage parameters or degradation variables, denoted as dc/dt. These variables range from zero for an undamaged material to one for complete damage. It is generally not advisable to use damage variables exceeding 0.99.

The compressive parameter, d_c, is expressed as $1 - \sigma / \sigma_{max}$, where σ_{max} equals the mean compressive strength f_{cm}. On the other hand, the tensile parameter, d_t, is defined as the ratio between the cracking strain and the total strain.

Shear lag

Shear lag phenomenon is a significant consideration in the design and analysis of box girder bridges, impacting their structural behavior under various loading conditions. Here's a paraphrase:

Box girder bridges rely primarily on their top and bottom flanges (horizontal elements) and the web (vertical element connecting the flanges) to carry the main load. When subjected to shear forces, like those from traffic or wind, the cross-section experiences shear stresses.

Effects of Shear Lag

1. **Nonuniform Stress Distribution:** The stiffness disparity between the flanges and the web causes an uneven distribution of shear stress across the cross-section. The stiffer flanges bear a greater share of the shear force, while the contribution from the web is comparatively lower. This disparity is commonly referred to as the shear lag effect.

2. **Reduced Effective Section:** Not all parts of the cross-section effectively resist shear forces due to shear lag. As a result, the portion of the cross-section that effectively resists shear is smaller than the total area.

3. **Stress Concentration:** Shear stress tends to concentrate in specific regions, particularly at the junctions between the flanges and the web. These areas may experience stress concentrations, potentially leading to localized yielding or fatigue damage over time.

4. **Risk of Structural Instability:** In severe cases, the shear lag effect can provoke buckling or instability in the flanges, especially under high shear force conditions.

Understanding and mitigating these effects are crucial for ensuring the structural integrity and safety of box girder bridges in service.
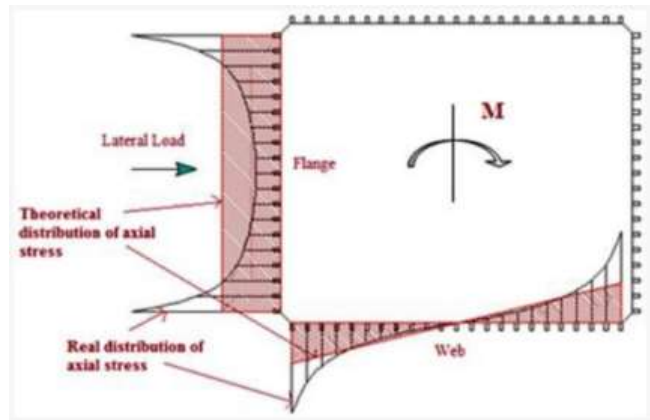
Figure 53-Axial stress distribution in the columns of the building in web as well as in flange panels.(Gaur & Goliya, 2015)

Validation of FEM

To ensure the utmost accuracy and robustness of the software's output, we embarked on a meticulous verification process. This involved the meticulous creation of a box girder model meticulously stripped of steel components and tendons, leaving a pristine framework for analysis. The section was ingeniously treated as a cantilever, with fixed boundary conditions meticulously applied to one of its faces, ensuring a stable foundation for examination.

To validate the software's performance, we didn't solely rely on its computations. Instead, we opted for a comprehensive approach, complementing the digital results with manual calculations. Focusing keenly on the displacement along the y-axis, we meticulously simulated the application of a point concentrated load at the extremity of the section, meticulously scrutinizing the ensuing response.

Moreover, our verification process extended to the examination of specific moment applications. We meticulously compared the software's predictions against our manual analyses, leaving no stone unturned in our quest for precision and reliability. By employing this rigorous methodology, we instilled confidence in the integrity of the software's data, ensuring its suitability for any critical engineering endeavor.

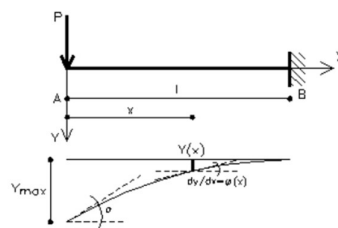Verification according to point concentrated load:

Figure 54- Cantilever beam.

From equation below, the equation of the elastic line of the analyzed beam is obtained:

$$y(x) = \frac{P}{6EJ}(x^3 - 3l^2x + 2l^3)$$

The maximum displacement occurs at the free end (x = 0). Substituting the value x = 0 into the equation above, we obtain:

$$y = \frac{Pl^3}{3EJ}$$
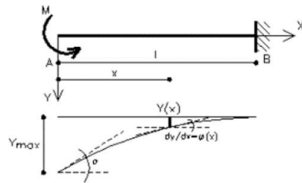
Verification according to applied moment:

Figure 55-Cantilever beam.

The equation of the elastic line of the analyzed beam is obtained:

$$y(x) = \frac{M}{2EJ}(x^2 - 2lx + l^2)$$

The maximum displacement occurs at the free end (x = 0). Substituting the value x = 0 into the equation above, we obtain:

$$y(x) = \frac{Ml^2}{2EJ}$$

Material input data :

Concrete:

Concrete Damage placticty (CDP) properties:

Using the above equations the following data was acquired and is used in abaqus.

Dilation angle	Eccentricity (ε)	$\sigma b0/\sigma c0$	Kc
31	0.1	1.16	0.67

Table 17

Compression behavior:

Total strain	Stress	inelastic strain	damage
ε_c (%)	σ_t (Mpa)	ε_c^{in}	d_c
0	0	-	-
0.0622	23.2	0	0
0.1083	36.606076	0.000101	0
0.1544	47.733488	0.000263	0
0.2004	55.211007	0.000523	0
0.2465	58	0.0009088	0
0.2672	57.355348	0.0011332	0.0111147
0.2879	55.301178	0.0013953	0.0465314
0.3086	51.630714	0.0017008	0.1098153
0.3293	46.094655	0.0020564	0.2052646
0.35	38.389653	0.0024702	0.3381094
0.615	20.384957	0.0056032	0.6485352
0.88	14.165575	0.00842	0.755766

1.145	10.15731	0.0111775	0.824874
1.41	7.3822411	0.013902	0.87272
1.675	5.4417969	0.016604	0.9061759
1.94	4.1212386	0.0192894	0.9289442
2.205	3.2866812	0.0219618	0.9433331
3	2.9	0.0299222	0.95
10	0.4	0.0999893	0.9931034

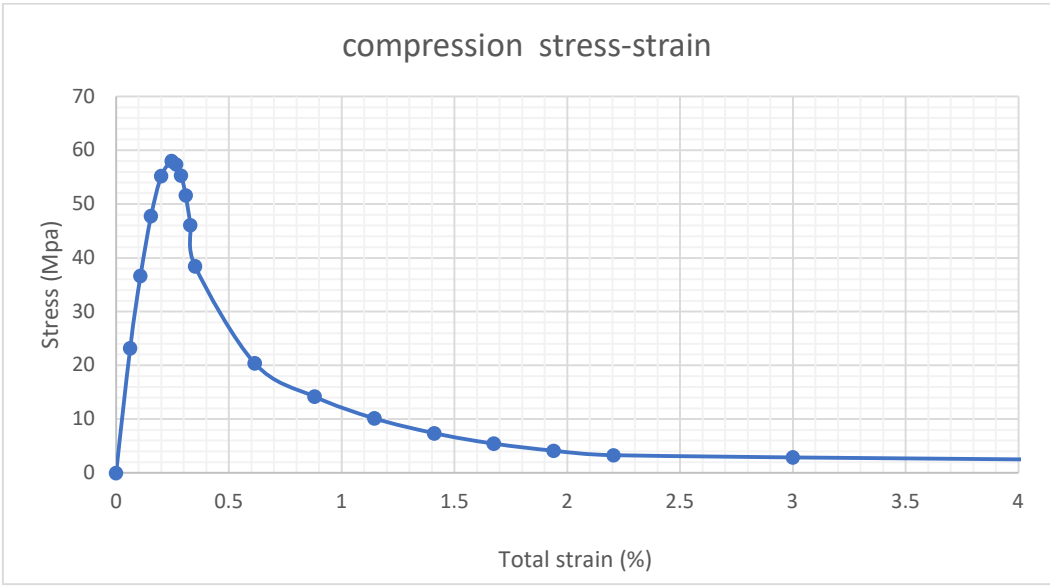Table 18- Concrete compressive behavior

Figure 56-Compression stress/strain curve.

Based on the provided stress-strain curve, it is evident that the concrete exhibits a maximum compressive strength of 58 MPa. This occurs at a corresponding maximum strain value of 0.0009088. Understanding these material properties is crucial for assessing the structural behavior of the concrete element under various loading conditions. By identifying the maximum compressive strength and corresponding strain, we gain valuable insights into the material's capacity to withstand compressive loads before reaching failure. This information informs the design and analysis processes, guiding decisions related to structural performance and safety.

Tensile behavior:

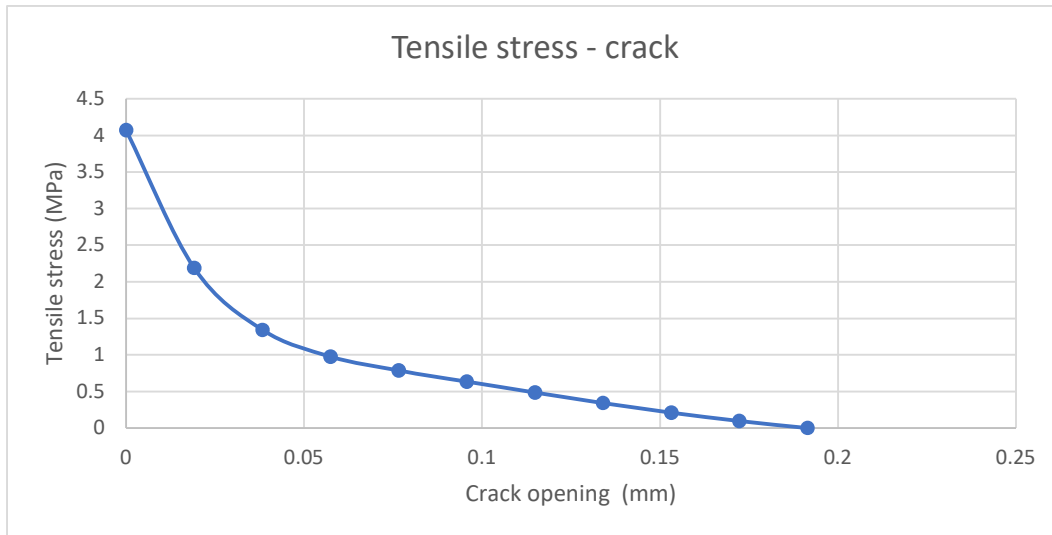| Crack displacement	Stress	Damage
W (mm)	σ_t (Mpa)	$(1-\sigma_t/f_t)$
0	4.071626	0.0000
0.019139699	2.187978	0.4626
0.038279397	1.34108	0.6706
0.057419096	0.977792	0.7599
0.076558794	0.785564	0.8071
0.095698493	0.634086	0.8443
0.114838191	0.486695	0.8805
0.13397789	0.342893	0.9158
0.153117589	0.210532	0.9483
0.172257287	0.095568	0.9765
0.191396986	0	1.0000

Table 19- Concrete Tensile behavior.

Figure 57-Tensile stress/crack curve.

Based on the provided tensile stress-crack opening curve, it appears that the concrete exhibits a maximum tensile stress of 4.07 MPa at a crack opening of 0 mm. This indicates the concrete's ability to resist tensile stresses up to this threshold value before experiencing cracking. Understanding this behavior is crucial for assessing the structural response of concrete elements, particularly in applications where tensile forces may be present.

5.2 Geometric model:

In the geometric modeling phase, the concrete section of the box girder was meticulously recreated as a 3D deformable solid component within the finite element model in Abaqus. Each reinforcement and tendon element was also meticulously drawn according to the detailed design drawings, accurately representing their positions and dimensions. While the concrete was modeled as a 3D deformable solid component, the reinforcement and tendons were represented as 2D truss elements. This comprehensive approach ensured that the finite element model faithfully reflected the structural composition and geometry of the box girder, setting a solid foundation for subsequent analyses.
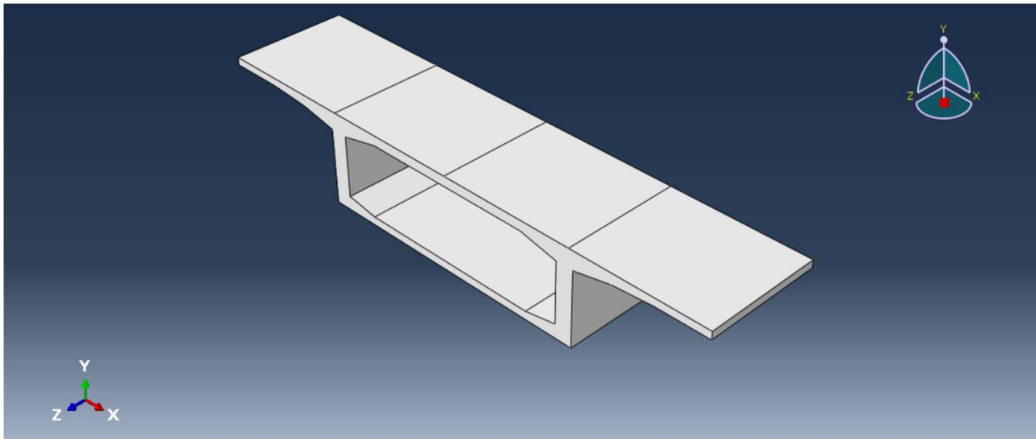

Figure 58- Geometric model.

Assembly

In the assembly phase within Abaqus, we meticulously constructed the entire girder section, integrating both reinforcement steel and tendons according to the design specifications and drawings. Paying close attention to the distribution of reinforcement as per the design, we ensured precise alignment and placement of components within the assembly. This meticulous assembly process laid the foundation for an accurate representation of the girder's behavior under various loading conditions in the subsequent finite element analysis.
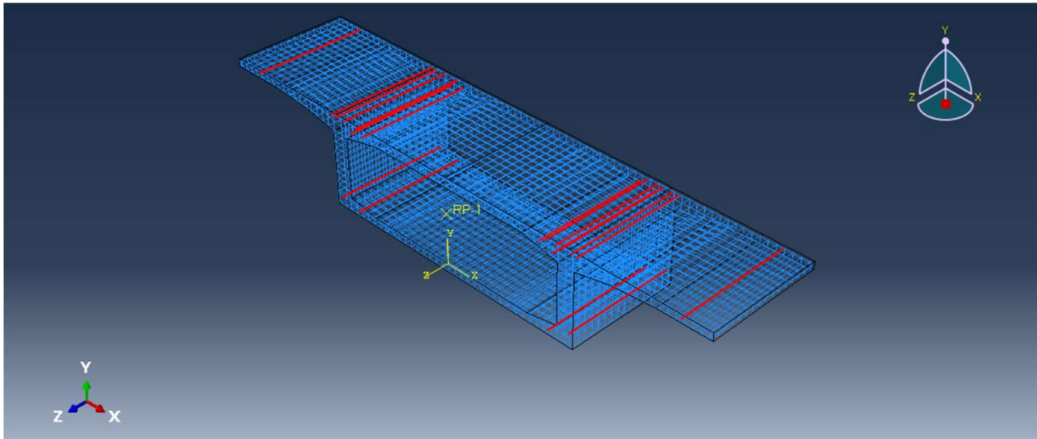
Figure 59-Assembly of model.

Step

The finite element model in Abaqus utilized a static, general step to analyze the behavior of the reinforced concrete section. This step was chosen to simulate the structural response under static loading conditions, allowing for the accurate prediction of stresses, strains, and deformations within the concrete section. By employing this analysis approach, we were able to assess the structural performance and integrity of the reinforced concrete element under typical loading scenarios.
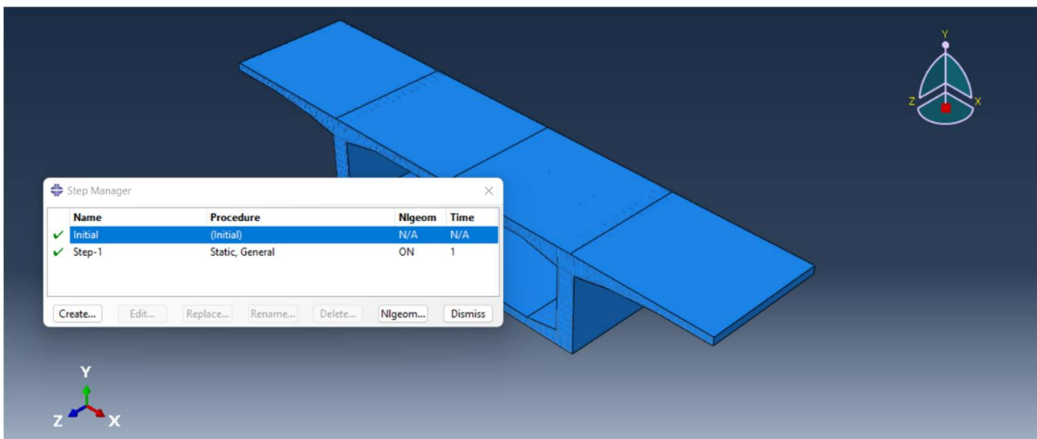

Figure 60-static, general step

Interaction

In the finite element analysis conducted in Abaqus, I employed the embedded region feature to accurately model the interaction between reinforcement steel and tendons within the concrete structure. By defining embedded regions for these components, I was able to simulate their behavior within the concrete matrix, capturing their influence on the overall structural response with precision and realism.
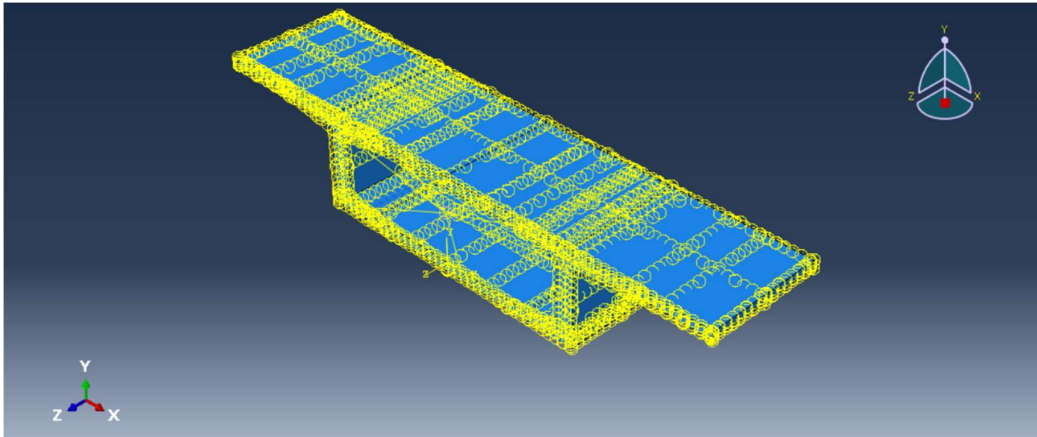

Figure 61- Interaction between concrete and steel

Kinematic coupling in Abaqus is a powerful tool for modeling complex interactions between components with prescribed motions or constraints. It's particularly useful in scenarios where parts need to move together in a specific manner or where certain degrees of freedom need to be constrained.

With kinematic coupling, you can define relationships between different parts or surfaces in terms of relative motion or constraint conditions. This allows you to simulate interactions such as sliding, rolling, or rotating between components accurately.
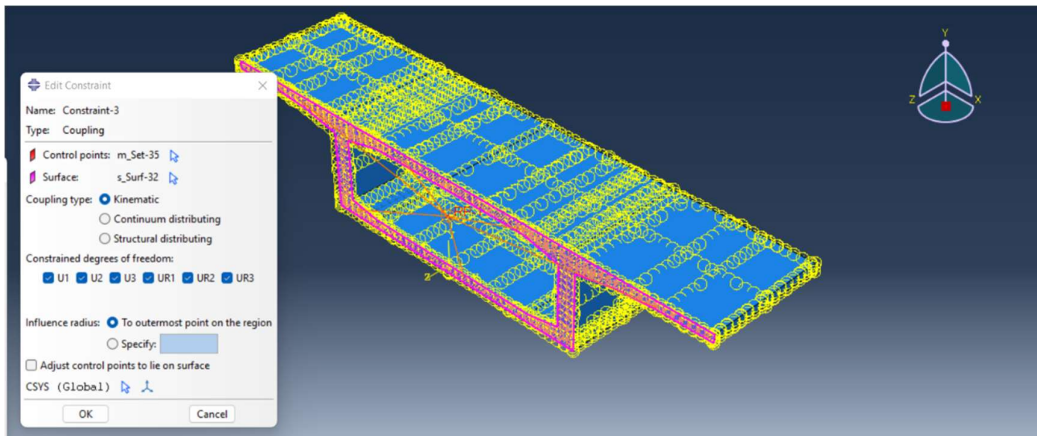

Figure 62- Coupling constraint.

Boundary conditions

For the boundary conditions, we applied a comprehensive fixed constraint to one of the faces of the model. This choice was deliberate, as the section under study is situated closest to the abutment, bearing a significant counterweight load. Therefore, to accurately simulate the real-world scenario, we deemed it appropriate to immobilize the surface in contact with the abutment entirely. This boundary condition modeling was executed meticulously within the Abaqus environment, ensuring that the structural response at this critical interface was appropriately captured in the subsequent analyses.
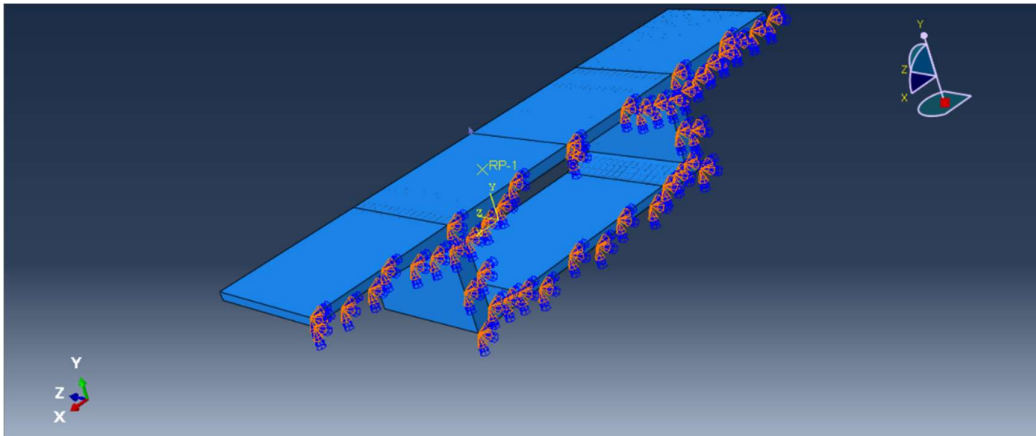

Figure 63-Boundary conditions.

Applied loads

In the load application phase within Abaqus, a jacking force of 1360 MPa was meticulously applied to the tendons as a predefined load. This specific force was chosen in accordance with the design requirements and specifications. By accurately applying the jacking force to the tendons, we ensured that the finite element model faithfully represented the expected loading conditions, allowing for a comprehensive analysis of the structural response under the specified loads.
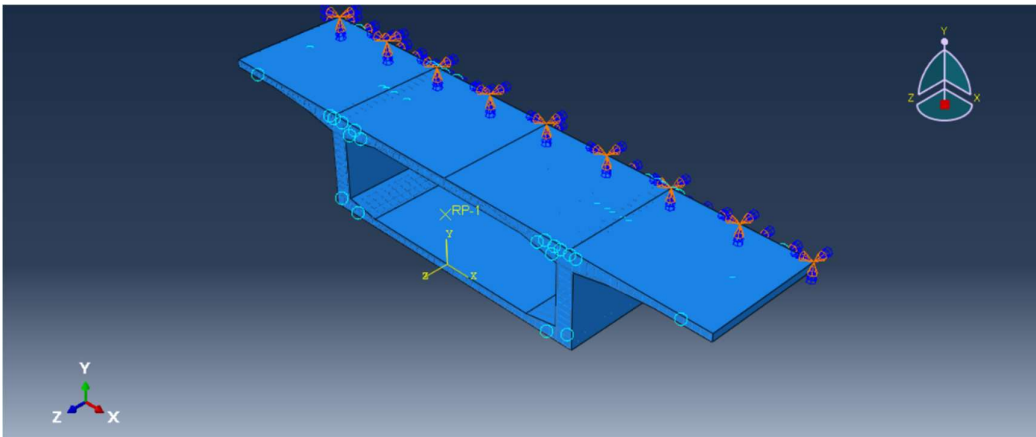

Figure 64- jacking force of the tendons.

In the loading phase of the analysis, the load was applied to the section through the reference point XRP-1. The reaction values from the entire model, obtained from MIDAS, were meticulously incorporated into the Abaqus simulation. This included torsional forces acting on all axes (x, y, z) as well as shear forces acting on all axes (x, y, z). By accurately applying these reaction values in Abaqus, we ensured that the finite element model was subjected to realistic loading conditions, allowing for a comprehensive assessment of the structural response under the specified loads.
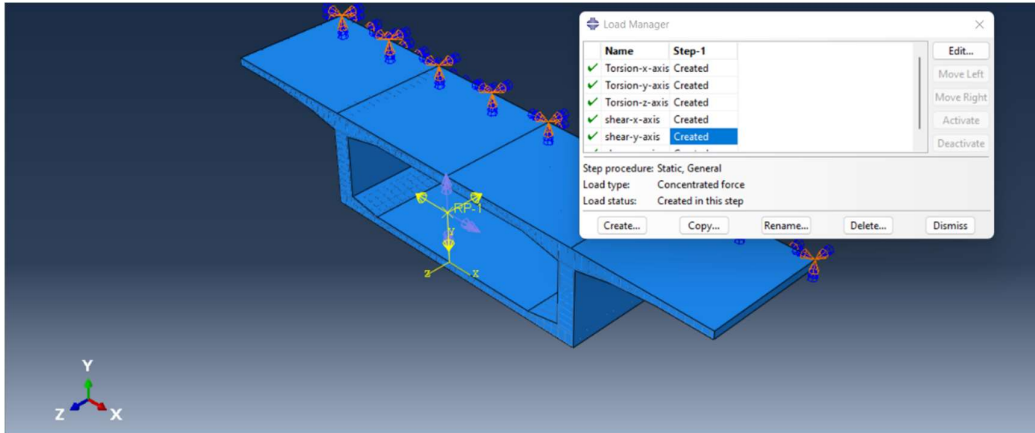

Figure 65- Applying Loads.

Mesh:

In the meshing phase within Abaqus, each part of the section, including the steel, tendons, and concrete components, was meticulously meshed individually. A global mesh size of approximately 200 was selected for this purpose. This mesh size was chosen to strike a balance between computational efficiency and mesh accuracy. By meshing each part separately, we ensured that the finite element model accurately represented the geometric intricacies and material heterogeneities of the entire structure. This approach facilitated a detailed analysis of the structural response while optimizing computational resources in Abaqus.
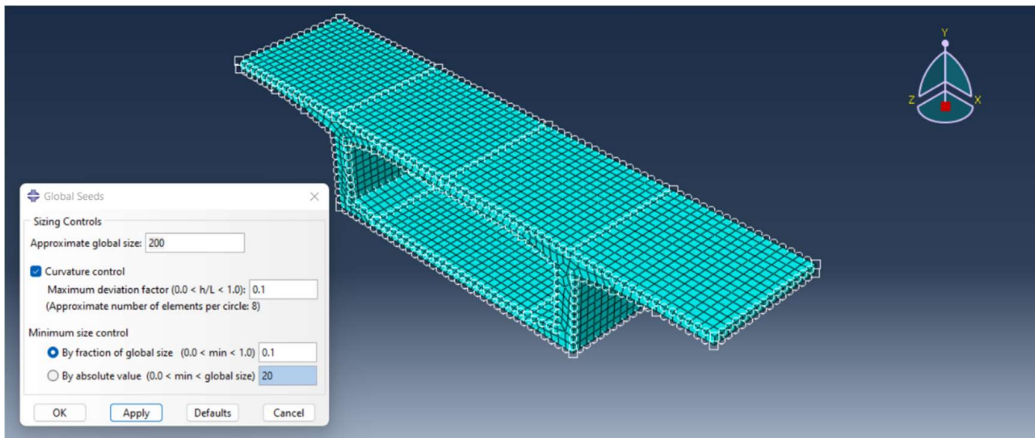

Figure 66- Mesh of concrete section.

5.3 Reaction forces from midas applied in abaqus model:

In our modeling process, we utilized a global model for the entire bridge designed in MIDAS software. This comprehensive model enabled us to analyze the forces acting on our specific box-girder section within the context of the entire bridge structure. To accurately represent these forces in our Abaqus simulation, we established a reference point at the centroid of the section. By doing so, we ensured that the loads applied to the section in Abaqus were representative of the forces derived from the global model. This approach was essential for simulating realistic loading conditions and ensuring the structural integrity and performance of the section within the broader bridge context.
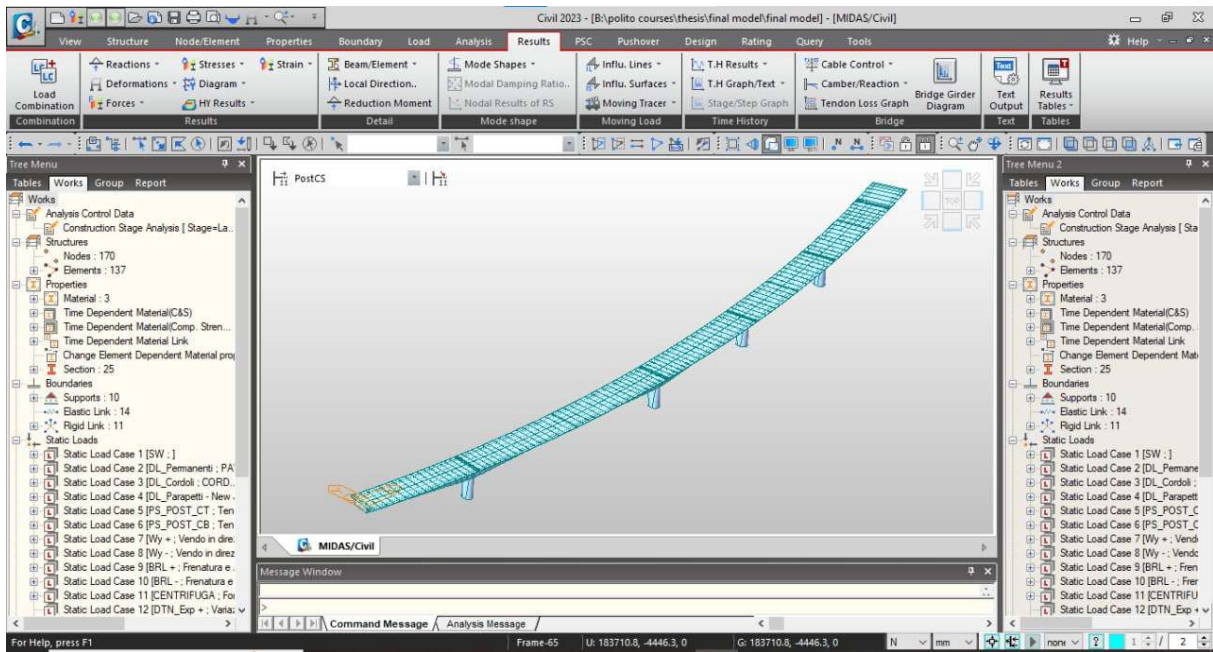

Figure 67- Midas model.

Incorporating the torsion and shear forces obtained from MIDAS into our Abaqus simulation was a crucial step in accurately representing the loading conditions on our section. These forces were meticulously applied as loads to our section within Abaqus. By doing so, we ensured that the finite element model captured the real-world behavior of the structure under the influence of torsional and shear loading. This comprehensive approach allowed us to assess the structural response of our section with precision, considering the effects of these critical loading components derived from the global model.

Elem	Load	Part	Axial (N)	Shear-y (N)	Shear-z (N)	Torsion (N·mm)	Moment-y (N·mm)	Moment-z (N·mm)
124	ali	I[124]	4094.70	-73339.37	7077217.16	2611008840.40	-24201849643.75	1625196153.57
124	ali	J[125]	4094.70	-73339.37	8069751.83	2805883300.40	-43903834884.12	1815882686.51

Figure 68- Acting shear and torsion on our section.

Applying these forces in our model on abaqus.
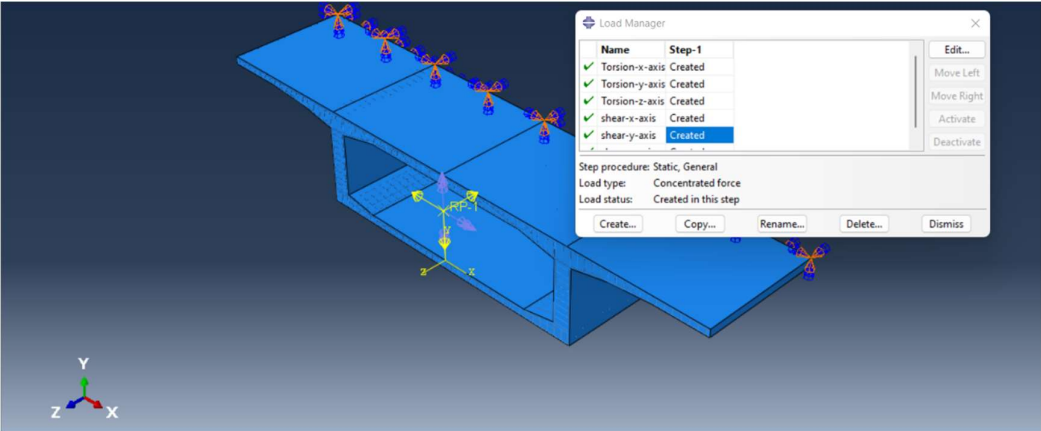

Figure 69- Applying the shear and torsion.

6 RESULTS:

6.1 Results from the detailed model in Abaqus:

Max stress principle:

In the provided image, the response of the maximum stress in the concrete due to loading is visually depicted. Additionally, the stress distribution across various points of the section is illustrated, showcasing the granularity of the meshing strategy employed. This comprehensive meshing approach enabled us to capture localized stress variations within the concrete element, providing valuable insights into its structural behavior under the applied loads. By visualizing stress distribution at individual points, we gained a deeper understanding of how the structure responds.

Figure 70- Max principal stresses.
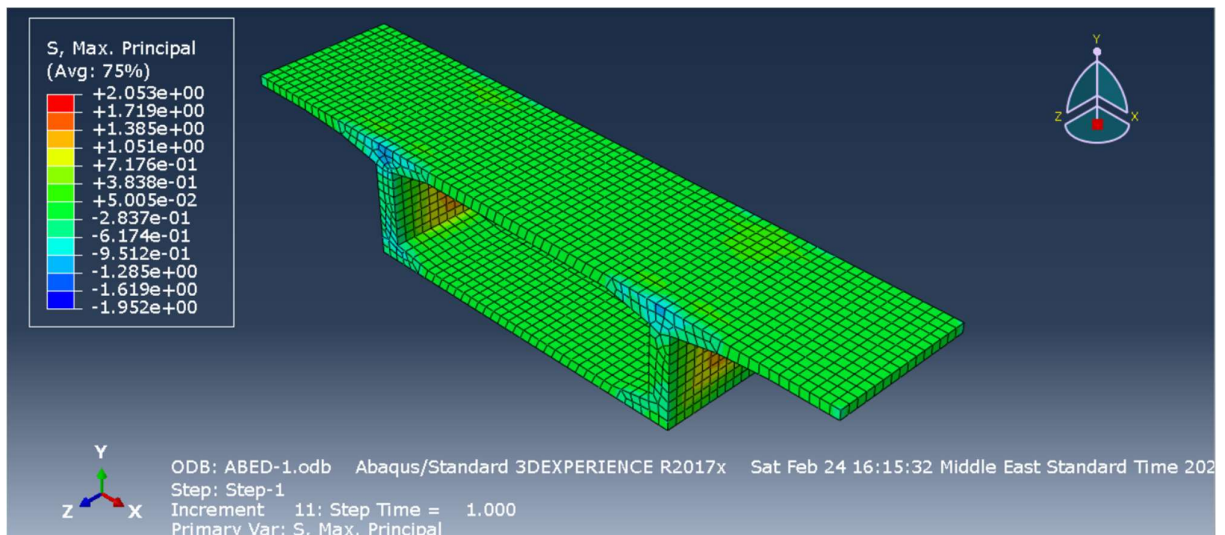
The observation of maximum stress concentration within the webs of the girder, ranging approximately between 1.38 and 2.053 MPa, is significant. This finding highlights the critical areas where the structural elements experience the highest stress levels under the applied loading conditions. Identifying these stress concentrations allows us to focus on potential areas of concern
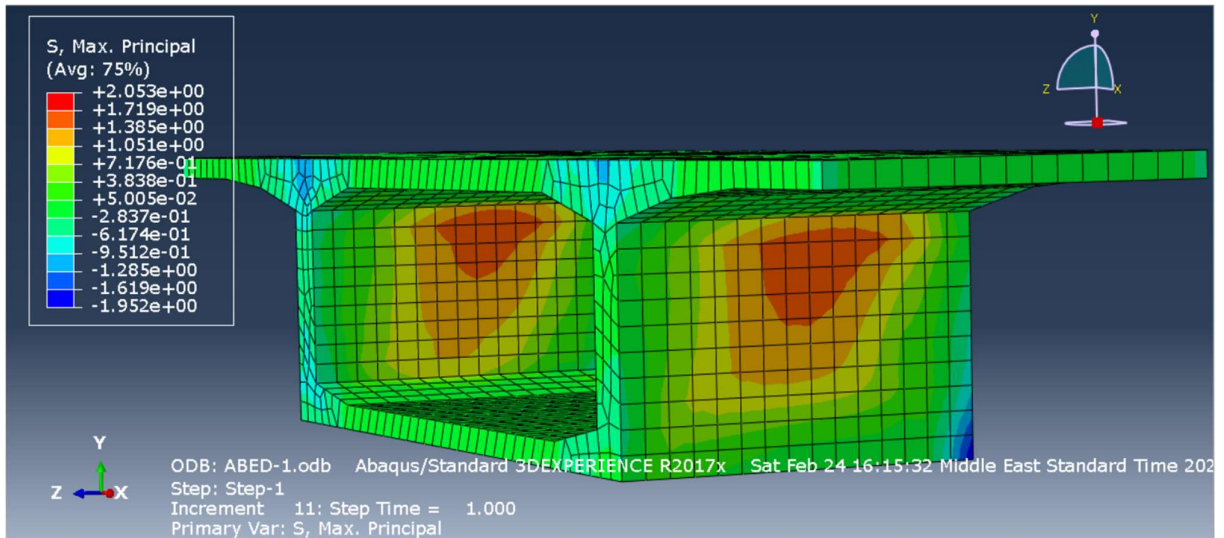
Figure 71- Detail of Max principal stresses.

Displacement output

The analysis of displacement in the provided figure reveals crucial insights into the structural behavior under loading conditions. It is evident that the maximum displacement occurs at the free surface of the structure, where there are no boundary conditions allowing for greater movement. Conversely, at the face with fixed boundary conditions, the displacement is effectively zero, as expected. The recorded maximum displacement of 2.7 mm.

Figure 72- Combined displacement in the three directions (X, Y, Z).

6.2   Discusion of the results:

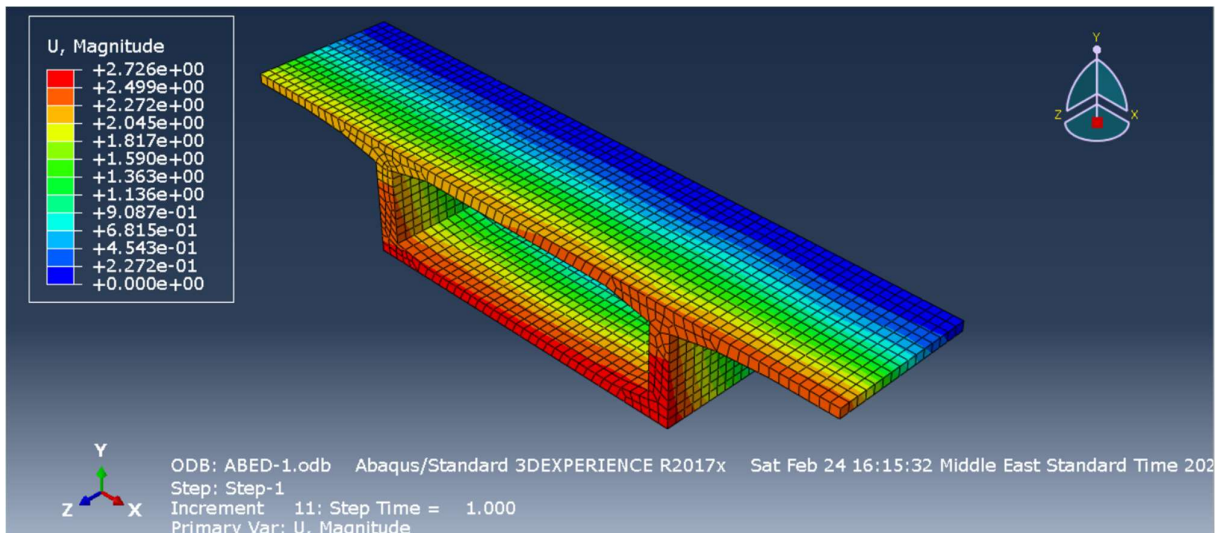We aim to compare the observed crack widths during on-site inspections with the stress results obtained from Abaqus simulations. By doing so, we seek to determine if the observed crack openings match the stress-induced crack formations predicted by our analysis, thereby discerning the underlying causes of the cracks.

During on-site inspections, the widest crack measured was 1.2 mm. In our study, based on concrete damage plasticity analysis, we established that cracks start forming when the tensile stress in the section reaches 4.07 MPa. Our Abaqus simulations, conducted under serviceability limit state (SLS) conditions, indicate that the stress in the section has not exceeded 4.07 MPa. This suggests that the cracks observed on the section cannot solely be attributed to concrete properties or the applied loads.

In essence, our findings imply that factors other than concrete properties or applied loads may be contributing to the observed crack formations. Further investigation is warranted to identify and address these additional factors influencing the structural integrity of the section.

7 *Conclusions:*

The investigation conducted in this thesis sheds light on the occurrence and behavior of cracks in post-tensioned bridges, with a particular emphasis on structures subjected to tensioning forces. Through comprehensive finite element analysis, we simulated and analyzed the complex processes involved in crack formation and propagation within various components of post-tensioned bridge systems.

By adopting a simulation approach, this research significantly advances our understanding of crack development, facilitating a more precise assessment of the structural performance and safety of post-tensioned bridges. The utilization of advanced computational techniques allowed for an in-depth exploration of the interactions between design parameters, construction practices, material properties, and external forces, all of which influence crack initiation and propagation.

The insights gleaned from these simulations provide valuable contributions to the underlying mechanics of cracks in post-tensioned bridges. Such knowledge is crucial for informing the development of effective strategies for the design, maintenance, and rehabilitation of these critical infrastructure assets. Engineers and practitioners can leverage these insights to make informed decisions aimed at enhancing the resilience and longevity of post-tensioned bridge structures, thereby ensuring the safety and reliability of transportation networks on a global scale.

In conclusion, this thesis contributes to advancing the field of structural engineering by providing a comprehensive understanding of crack behavior in post-tensioned bridges and offering practical insights for improving their performance and safety in real-world applications. Further research and development in this area are essential for continuously enhancing the integrity and durability of transportation infrastructure worldwide.

8   References:

[1] Minh, Hoang-Le, et al. "A concrete damage plasticity model for predicting the effects of compressive high-strength concrete under static and dynamic loads." *Journal of Building Engineering* 44 (2021): 103239.

[2] Sümer, Yusuf, and Muharrem Aktaş. "Defining parameters for concrete damage plasticity model." *Challenge Journal of Structural Mechanics* 1.3 (2015): 149-155.

[3] Podolny, Walter. "The cause of cracking in post-tensioned concrete box girder bridges and retrofit procedures." *Pci Journal* 30.2 (1985): 82-139.

[4] Menga, Antonia, et al. "Corrosion-induced damages and failures of posttensioned bridges: A literature review." *Structural Concrete* 24.1 (2023): 84-99.

[5] Agredo Chavez, Angelica Maria, et al. "Cracking and Fatigue of Heavy Loaded Prestressed Concrete Bridge in Sweden." *IABSE Symposium Prague 2022: Challenges for Existing and Oncoming Structures, Prague, Czech Republic, May 25-27, 2022*. International Association for Bridge and Structural Engineering, 2022.

[6] Elgazzar, Hesham, and Viktor Ansnaes. "Concrete Cracks in Composite Bridges: A Case Study of the Bothnia Line Railway Bridge over Ångermanälven." (2012).

[7] Hafezolghorani, Milad, et al. "Simplified damage plasticity model for concrete." *Structural engineering international* 27.1 (2017): 68-78.

[8] PrimeC. (2017, May 31). 3 Methods for Crack Depth Measurement in Concrete. fPrimeC. Retrieved [Insert Access Date], from https://www.fprimec.com/3-methods-crack-depth-measurement-in-concrete/

[9] MIDAS. (n.d.). Traffic Load Consideration to Different Types of Bridges. MIDAS Blog. Retrieved \[Insert Access Date\]

[10] Cairo, Pier Paolo. *Application of BIM methodology for long steel deck bridge*. Diss. Politecnico di Torino, 2020.

[11] Oliva, Michael G., and Okumus Pinar. *Finite element analysis of deep wide-flanged prestressed girders to understand and control end cracking*. Wisconsin Highway Research Program, 2011.

[12] Le Thanh, Cuong, Hoang-Le Minh, and Thanh Sang-To. "A nonlinear concrete damaged plasticity model for simulation reinforced concrete structures using ABAQUS." *Frattura ed Integrità Strutturale* 16.59 (2022): 232-242.

[13] Tabatabai, Habib, and Azam Nabizadeh. *Strength and Serviceability of Damaged Prestressed Girders*. No. 0092-17-02. University of Wisconsin--Milwaukee, 2019.

[14] Raza, Ali, and Afaq Ahmad. "Numerical investigation of load-carrying capacity of GFRP-reinforced rectangular concrete members using CDP model in ABAQUS." *Advances in Civil Engineering* 2019 (2019).

[15] Code, Model. "fib model Code for concrete structures." *Structural Concrete* 14 (2010).

[16] Standard, British. "Eurocode 2: Design of concrete structures—." *Part* 1.1 (2004): 230.

[17] Yosef Nezhad Arya, Nessa. "Second-order FE Analysis of Axial Loaded Concrete Members According to Eurocode 2." (2015).S

[18] Dalbiso, Alemayehu Darge. "STUDY OF SHEAR LAG EFFECT IN BOX GIRDER BRIDGES." (2013).

[19] Gaur, Himanshu, and Ravindra Kumar Goliya. "Correlating Stiffness and Shear Lag Behavior with Brace Configuration of Tall Truss Tube Buildings." Buildings 5.3 (2015): 736-750.

[20] Williams, Alan. "Structural analysis: in theory and practice." (2009).

[21] Bouassida, Yorsa, et al. "Bridge design to Eurocodes-Worked examples." Work.''Bridge Des. to Eurocodes," Vienna (2012): 4-6.

[22] Petrangeli, Mario Paolo. Progettazione e costruzione di ponti: con cenni di patologia e diagnostica delle opere esistenti. Masson, 1996

[23] Hurlebaus, Stefan, et al. "Condition assessment of bridge post-tensioning and stay cable systems using NDE methods." Transportation Research Board of the National Academies, Texas A&M Transportation Institute: College Station, TX, USA (2016).

[24] Fülöp, Ludovic, et al. "Assessing the challenges of condition assessment of steel-concrete (SC) composite elements using NDE." Case Studies in Construction Materials 16 (2022): e00887.

[25] Saad, Timothy, et al. "Development of a Fatigue Life Assessment Model for Pairing Fatigue Damage Prognoses with Bridge Management Systems." Bridge Optimization-Inspection and Condition Monitoring. IntechOpen, 2018.

[26] Zhang, Guojing, et al. "Causes and statistical characteristics of bridge failures: A review." Journal of traffic and transportation engineering (English edition) 9.3 (2022): 388-406.

[27] EN, BS. "2: 2003, Eurocode 1: Actions on structures-Part 2: Traffic loads on bridges." ICS. Vol. 91. No. 30. 1991.

[28] e dei Trasporti, Ministero delle Infrastrutture. "Norme tecniche per le costruzioni." Ministero delle Infrastrutture e dei Trasporti, Decreto Ministeriale del 14 (2008).

[29] Wassef, Wagdy G., et al. Comprehensive Design Example for Prestressed Concrete (PSC) Girder Superstructure Bridge with Commentary (in US Customary Units). No. FHWA-NHI-04-043. United States. Federal Highway Administration, 2003.

[30] Janamian, Kambiz, and José B. Aguiar. Concrete Materials and Technology: A Practical Guide. CRC Press, 2023.

[31] Soltani, Arash, et al. "Empirical assessment and refinement of corrosion distribution models in the perimeter of corroded steel rebar subjected to chloride ions attack." Case Studies in Construction Materials 17 (2022): e01398.